frontiers in Energy Research

REVIEW
published: 24 March 2021
doi: 10.3389/fenrg.2021.651386

Mechanisms and Product Options of Magnesiothermic Reduction of Silica to Silicon for Lithium-Ion Battery Applications

Yu Tan[1], Tingting Jiang[1] and George Z. Chen[2]**

[1] The State Key Laboratory of Refractories and Metallurgy, College of Materials and Metallurgy, Wuhan University of Science and Technology, Wuhan, China, [2] Department of Chemical and Environmental Engineering, Faculty of Engineering, University of Nottingham, Nottingham, United Kingdom

Lithium-ion batteries (LIBs) have been one of the most predominant rechargeable power sources due to their high energy/power density and long cycle life. As one of the most promising candidates for the new generation negative electrode materials in LIBs, silicon has the advantages of high specific capacity, a lithiation potential range close to that of lithium deposition, and rich abundance in the earth's crust. However, the commercial use of silicon in LIBs is still limited by the short cycle life and poor rate performance due to the severe volume change during Li^{++} insertion/extraction, as well as the unsatisfactory conduction of electron and Li^{+} through silicon matrix. Therefore, many efforts have been made to control and stabilize the structures of silicon. Magnesiothermic reduction has been extensively demonstrated as a promising process for making porous silicon with micro- or nanosized structures for better electrochemical performance in LIBs. This article provides a brief but critical overview of magnesiothermic reduction under various conditions in several aspects, including the thermodynamics and mechanism of the reaction, the influences of the precursor and reaction conditions on the dynamics of the reduction, and the interface control and its effect on the morphology as well as the final performance of the silicon. These outcomes will bring about a clearer vision and better understanding on the production of silicon by magnesiothermic reduction for LIBs application.

Keywords: silicon, negative electrode, magnesiothermic reduction, lithium-ion batteries, interface control

OPEN ACCESS

Edited by:
Xiangming He,
Tsinghua University, China

Reviewed by:
Jianyu Huang,
Yanshan University, China
Zhaoping Liu,
Ningbo Institute of Materials Technology & Engineering (CAS), China
Xifei Li,
Xi'an University of Technology, China
Xiqian Yu,
Institute of Physics (CAS), China

****Correspondence:***
Tingting Jiang
ttjiang@wust.edu.cn
George Z. Chen
george.chen@nottingham.ac.uk

Specialty section:
This article was submitted to Electrochemical Energy Conversion and Storage, a section of the journal Frontiers in Energy Research

Received: *09 January 2021*
Accepted: *01 March 2021*
Published: *24 March 2021*

Citation:
Tan Y, Jiang T and Chen GZ (2021) Mechanisms and Product Options of Magnesiothermic Reduction of Silica to Silicon for Lithium-Ion Battery Applications. Front. Energy Res. 9:651386. doi: 10.3389/fenrg.2021.651386

INTRODUCTION

Silicon-Based Negative Electrode Materials: Advantages and Challenges

The development of green and sustainable energy technologies has become one of the most important issues in the world facing the problems of energy and environment resulting from the massive use of fossil fuel based technologies. Clean energy technologies are widely investigated and being fast developed into both industrial and domestic applications. A good example is lithium-ion batteries (LIBs) which play a vital role in portable electrical devices for years and are being increasingly applied in electric vehicles and electricity storage banks. LIBs are currently leading their competitors in terms of several technical specifications, such as energy density (or driving range) and working lifetime. However, there are still challenging issues such as recharging rate,

cost and safety of LIB based power systems that are still limiting the market promotion of electric vehicles. Improved safety, higher energy density and lower cost are greatly desirable. The electrode materials in commercial LIBs are made of carbon-based materials for the negative electrode (negatrode) and lithium transition metal oxides for the positive electrode (positrode). Although graphite shows the advantages of a fairly wide potential range close to that of the Li^+/Li couple, high stability, and low cost, it cannot meet the continuously increasing requirement for higher energy and power density nowadays.

Silicon (Si) provides a dramatically higher lithium storage capacity than graphite and is regarded as one of the most promising candidates for next generation negatrode material. Besides, silicon has a working potential range comparable to that of graphite. Further, the high abundance, low cost and environmental friendliness of silicon make it accessible to mass application. During the lithiation process (charging), lithium and silicon would form a series of lithium silicides (Li_xSi_y, $x/y \leq 4$), which is quite different from the insertion of Li^+ ion into graphite layers. At the initial stage of lithiation, some of the Si-Si bonds in the matrix breaks, and the original crystalline Si gradually transfers into amorphous Li_xSi. With the progress of lithiation, the amorphous Li_xSi reacts with more Li^+ ions and crystallizes to $Li_{15}Si_4$ (Sun et al., 2016; Gao et al., 2017; Tornheim et al., 2019). The corresponding potential plateau is below 90 mV vs. Li/Li^+ (Obrovac and Krause, 2006; Gao et al., 2017; Tornheim et al., 2019). During the delithiation process (discharging), $Li_{15}Si_4$ changes back to Li_xSi and finally becomes amorphous Si. In the subsequent lithiation and delithiation cycles, conversions only happen between Li_xSi and amorphous Si (Obrovac and Krause, 2007).

This article will mainly focus on magnesiothermic reduction (MTR). In the following sections, the preparation methods of silicon for LIBs, the reaction mechanism of MTR, the interface control and the application of silicon from MTR in LIBs are reviewed. Several methods to produce silicon negatrodes have been compared firstly. Then, the mechanisms of MTR and side reactions under various conditions are discussed, including the reaction process, by-products, and the influences of the precursor and reaction conditions on the dynamics. As the most promising candidate for next generation negatrode materials, Si material should overcome the volume expansion and the accompanying pulverization for mass application. Si from reduction of silica by Mg generally presents a porous morphology, which can provide the buffer space for expansion and hence a better cycle performance. The battery performances of these nanostructured Si are compared and identified. However, the yield and repeatability in MTR should be noticed. The final part presents the conclusions and perspectives of magnesiothermic reduction in large-scale negatrode material applications.

Preparation Methods of Silicon-Based Negative Electrode Materials

Up to now, there are several problems with using Si as the negatrode material in LIBs (Yao et al., 2011). These problems can be categorized into internal and external challenges. The internal challenges come from the intrinsic characteristics of Si (Liu et al., 2012; Li et al., 2015; Ashuri et al., 2016a). During the lithiation of Si, there is a volume expansion up to 300% (Sun et al., 2016). The severe expansion during lithiation and the consequent contraction in delithiation may lead to the pulverization and fracture of the Si based active material, and even peeling off the current collector, resulting in an irreversible capacity loss (Obrovac and Krause, 2007). In addition, as a semiconductor, Si has an electrical resistivity in the range of 10^{-4}–10^{10} Ω·cm at room temperature, depending on purity and doping. The low carrier transportation rate may affect the rate performance in LIBs. On the other hand, the external challenges are related to other compositions in LIBs. The electrode is composed of the copper foil current collector, active material, conductive additives and adhesives. In the working voltage range of LIBs, components in electrolyte are not stable and prone to decompose or react with Si. Then a film forms on the surface of Si based active material called solid electrolyte interphase (SEI) (Cho and Picraux, 2014; Stetson et al., 2019). The SEI formation on Si surface is different from that on the graphite surface. As an insulating layer, Si SEI consumes a large concentration of Li^+ ions and may impede the diffusion of Li^+ ion between Si and the electrolyte, leading to a low initial coulombic efficiency. In addition, crack and pulverization of Si after cycles would continually generate new surfaces of Si and hence new SEI. Thus, the SEI deteriorates both rate and cycling performance of Si due to this external issue.

To solve these problems, many efforts have been made in several aspects. Si negatrodes with micro morphology and structure have been designed. There is evidence showing that 150 nm is the critical size withstanding pulverization (Liu et al., 2012). Various Si-based nanomaterials and nanostructures have been developed, from 0D to 3D, including Si nanoparticles (SiNPs) (Chen et al., 2017), hollow particles (Yao et al., 2011), nanowires (Kumar et al., 2017; Jangid et al., 2018), nanorods (Chen et al., 2018a), nanotubes (Taeseup et al., 2010), core-shell (Kim J.S. et al., 2015; Lim et al., 2014), yolk-shell structures (Yang et al., 2015; Guo et al., 2017), and porous Si (Sohn et al., 2018). These structures could provide more buffering space for huge volume expansion and high mechanical stability to withstand stress, resulting a more constant structure and capacity. Another approach is combining Si with other materials of high stability and electrical conductivity like carbon, metal or metal oxides. Carbon materials (Terranova et al., 2014; Qi et al., 2020), including amorphous carbon (Hsu et al., 2020), graphene (Hsieh and Liu, 2020), graphite, carbon nanotubes, and fibers (Hieu et al., 2014; Chen et al., 2015; Cai et al., 2017; Liu et al., 2017; Kong et al., 2019), are the most researched ones, and carbon could always act as buffer layer for volume change of Si and increase the electrical conductivity of the whole composite. Composites of Si and these materials integrate advantages of high charge capacity of Si and fast carrier transportation and mechanical properties of carbon materials. Therefore, Si-based composites are the most promising negatrodes for commercialisation due to its balanced good performance and relatively low cost. In addition to modification of Si materials, selection and incorporation of electrically conductive additives, binders, and electrolyte composition could also improve the performance

of Si-based negatrodes by solving the external challenges. The traditional binder polyvinylidene fluoride (PVDF) is proven to be not suitable for Si-based electrodes with a large volume expansion. Binders with higher adhesivity and ductility like carboxy methylated cellulose (CMC) have been adapted for Si-based materials (Buqa et al., 2006; Magasinski et al., 2010; Lim et al., 2015; Kierzek, 2016; Ma et al., 2020). Different from the commercial electrolytes for graphite, extra additives have been widely studied, aiming at helping the formation of a more stable SEI between the electrolyte and Si-based materials.

Chemically pure Si is utilized as a very important material in integrated circuit industry and renewable energy technologies. The Si manufacturing processes have been investigated thoroughly, few of which are mature, but many others are just emerging from laboratories, particularly those used to fabricate nano-structured Si negatrode materials as shown in **Figure 1**. Carbothermic reduction is the most well-known and frequently used strategy to reduce SiO_2 to the metallurgical Si (purity $\leq$ 98%). Carbon and high purity quartz react in the electric arc furnace at temperatures as high as 2,000°C. The received metallurgical Si can be widely used in alloy metallurgy, semiconductor industry and organosilicone chemical engineering. The higher purity electro-grade and solar-grade Si ingots can be obtained by the modified Siemens method or Czochralski method (Kawado et al., 1986; Yoshikawa and Morita, 2012; Zhilkashinova et al., 2018). Nanostructured Si, especially porous Si and Si nanowires can be produced by etching Si wafers in an HF or alkaline solution. However, this process is very energy intensive, expensive and with massive contaminating emissions.

Chemical vapour deposition (CVD) has proven to be a very effective route to fabrication of nanostructured Si with various kinds of morphologies including nano spheres, nano sheets, nano wires, nano tubes, and thin films. Nano Si materials prepared by CVD always present excellent electrochemical performances, but the precursor silane (SiH_4) in this method is highly toxic, easily pyrophoric and expensive (Yao et al., 2011). On the other hand, the costly equipment, complex production process, and a very low production yield all limit the scale production of nano Si by CVD.

Another route is the electrochemical reduction of Si in molten salt, which could realize relatively high purity Si products with morphology-controllable nanostructures at lower temperatures (generally 650–900°C) in comparison with the carbothermic reduction method (Jiang et al., 2020). The production yield and efficiency are the biggest problems which limit its commercial application.

Metallothermic Reduction of Silica

According to the Ellingham diagram in **Figure 2A**, ΔG^o of the reaction of Si with oxygen is fairly negative in the whole temperature region from 273 to 2,200 K, indicating the high chemical stability of SiO_2. The oxidation of sodium (Na), lithium (Li), aluminium (Al), magnesium (Mg), and calcium (Ca) all present a more negative value of ΔG^o than the oxidation of Si. Therefore, these metals could act as the reductant for reduction of SiO_2 into Si. Among these metals, the use of Na and Li to thermally reduce silica is limited by high cost and extreme reactivities. Ca is a good reductant in thermodynamics, but preparation of pure Ca needs expensive and complex technology. In a comprehensive consideration, Mg and Al are more suitable reductants to reduce silica to Si due to lower temperatures, faster processes and higher Si yields. Mechanisms in silica reduction by Mg and Al are similar according to Eqs. 1 and 2, both of which are solid-gas interface reactions.

$$3SiO_2(s)4Al(l) \rightarrow 2Si(s)2Al_2O_3(s) \quad (1)$$

$$SiO_2(s)2Mg(g) \rightarrow Si(s)2MgO(s) \quad (2)$$

Molten aluminum reacts with silica to produce silicon or Al-Si alloys. However, Al_2O_3 produced in aluminothermic reduction, i.e., Reaction (1), is chemically more inert than MgO, and may impede the subsequent reduction, leading to a high concentration of unreduced silica (Kui et al., 2001; Entwistle et al., 2018; Xing et al., 2018). Mg is mixed with SiO_2 and the temperature rises until Mg melts and starts to vaporize. As a highly exothermic reaction, magnesiothermic reduction can operate at a lower temperature around 650°C than aluminothermic reduction, indicating a better morphology control of the final product.

As a simple single-step method at relatively low temperatures (∼650°C), MTR can maintain the micro morphology of precursors. Numerous works have focused on nanostructured Si prepared by MTR under various conditions with different SiO_2 precursors. The received Si materials displayed controllable morphology and excellent electrochemical performances as negatrodes in LIBs. Since 1980s when researchers found that MTR could reduce silica into Si (Gutman et al., 2006), various attempts have been conducted, including utilizing different precursors like sand or biomass materials. In 2012, Cui et al. (Liu et al., 2013) prepared SiNPs with a high reversible capacity and long cycle life by MTR using rice husks as the Si source. Qiu et al. (2014) synthesized porous Si spheres through magnesiothermic from SiO_2 sphere deriving by hydrolysis TEOS.

REACTION MECHANISM OF THE MAGNESIOTHERMIC REDUCTION OF SILICA

Reaction Mechanism and Process

According to the Mg-Si-O phase diagram in **Figure 2B**, SiO_2, Si, MgO, Mg_2Si, $MgSiO_3$, and $MgSiO_4$ are stable at room temperature. XRD analyses of the reduced products proved the existence of Si, MgO, Mg_2Si, $MgSiO_3$, Mg_2SiO_4, and as well as the unreacted SiO_2 (McHale et al., 1996). Other phases like SiO generated during the MTR are thermodynamically unstable. Equation 2 is the ideal reaction, but other side reactions may occur, leading to quite a few by-products. The nature of the precursor and reaction conditions may affect the reduction process, the number of by-products and the yield of Si. Therefore, there has not yet an agreement on the exact and detailed reaction mechanism of MTR. In general, the reaction is promoted by

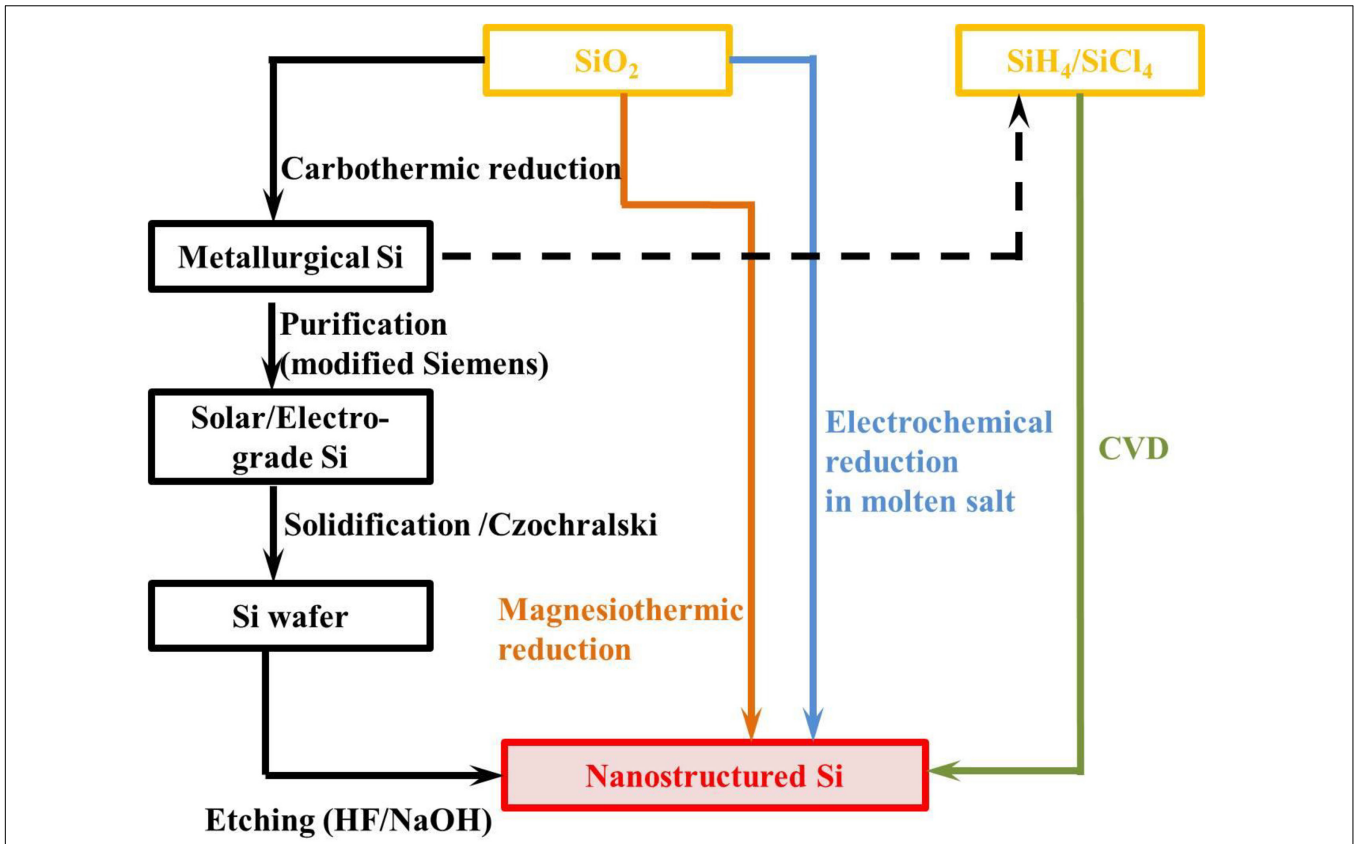

FIGURE 1 | Schematic diagram of the preparation of nanostructured silicon via different routes.

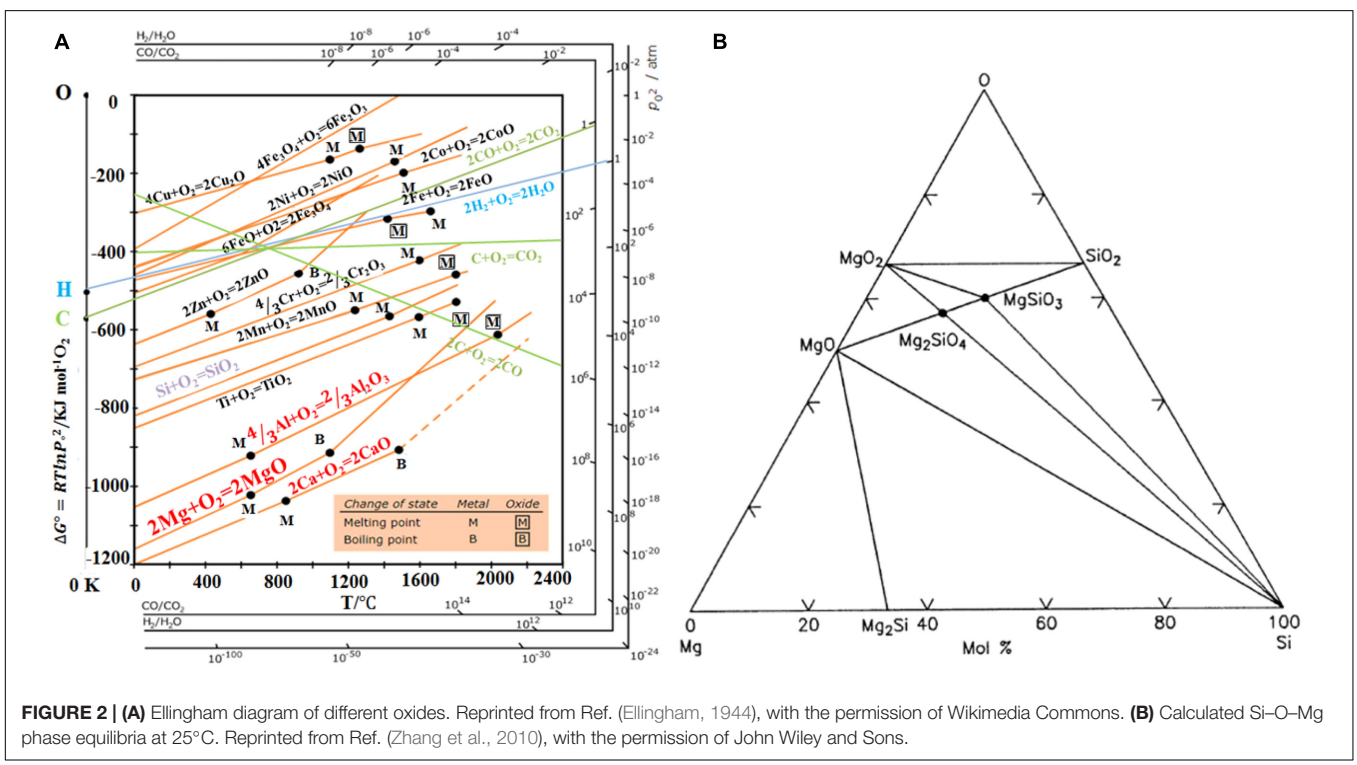

FIGURE 2 | (A) Ellingham diagram of different oxides. Reprinted from Ref. (Ellingham, 1944), with the permission of Wikimedia Commons. **(B)** Calculated Si–O–Mg phase equilibria at 25°C. Reprinted from Ref. (Zhang et al., 2010), with the permission of John Wiley and Sons.

mixing Mg and SiO_2 powers. Heating the mixture in a furnace under an inert or reducing atmosphere to temperatures above the melting point (648°C) of Mg, the Mg powder particles liquidize, generating a low pressure Mg vapor which reacts readily with adjacent solid SiO_2 powers. This gas-solid reaction is expected to be dominantly controlled by the diffusion of the Mg vapor in the gaps between the solid particles of SiO_2 and/or MgO. Under most conditions, the molar ratio Mg: SiO_2 is set to 2:1 to ensure a sufficiently large Si yield.

Figure 3A plots the variation of the mass fractions of different products from MTR against the reaction time which are calculated from XRD patterns in **Figure 3B**. At the initial stage, the Mg vapor only exists near the surface of SiO_2 and the pressure of Mg vapor is relatively high, then the near-surface SiO_2 can be reduced according to Eq. 2, for which $\Delta G^o = -245.2$ KJ mol^{-1} at 680°C. There is a large amount of heat release from MTR, leading to other undesired reactions, aggregation and structure collapse of the Si product. For example, if the precursor contains carbon, SiC will form in a local high-temperature region (Zuo et al., 2019). In a macro-view, SiO_2 is eroded by Mg, leaving Si and MgO in the matrix and with the outward diffusion of O (Ba et al., 2019). Meanwhile, the Mg vapor diffuses into SiO_2 continuously and a silicide will form at the Si and Mg interface according to Eq. 3 for which ΔG^o is −63.4 KJ mol^{-1} at 680°C.

$$Si(s)Mg(g) \rightarrow Mg2Si(s) \quad (3)$$

Product analyses at different reaction stages proved the high concentration of Mg_2Si at the first tens of minutes during reduction (Yoo et al., 2014; Zhang et al., 2014). A layered structure of $MgSi_2$/MgO was observed by I. Gutman (Gutman et al., 2006, 2009), suggesting the formation of Mg_2Si in the reduction process. However, Mg_2Si is not stable (Waitzinger et al., 2015) according to thermodynamics and may decompose to Si and Mg whilst the regenerated Mg may vaporize partly again at 850°C (Shepherd et al., 2008; Won et al., 2011). In most instances, Mg_2Si acts as an intermediate phase in MTR, which was formed at the beginning stage and then gradually disappear by reacting with SiO_2 following Eq. 4 whose ΔG^o is −181.8 KJ mol^{-1} at 680°C.

$$Mg_2Si(s)SiO_2(s) \rightarrow 2MgO(s)2Si(s) \quad (4)$$

As shown in the ternary Mg-Si-O phase diagram in **Figure 2B**, SiO_2 and Mg_2Si can hardly form a stable interface. Therefore MgO and Si may exist along with SiO_2. According to the step-by-step phase analysis of the products at different reaction times, the mass fraction of Mg_2Si was found to be several times higher than that of Si at the early stage of the reduction (10 min), while the amount of Mg_2Si dropped quickly and those of Si and MgO increased later (Yoo et al., 2014). Therefore, the silicide formation dominates the reduction process at the initial stage when the Mg vapor pressure is relatively high near the surface of SiO_2. Reaction (4) happens immediately following the formation of Mg_2Si except for the surface region where SiO_2 hardly remains. At later stages of the reduction, the signal of Mg_2Si is much weaker on the XRD patterns and most Mg_2Si exists only at the surface region.

Upon exposure to the inward diffusing Mg vapor, SiO_2 could be reduced by Mg and Mg_2Si gradually, leaving Si and MgO as the products (**Figure 3C**). The reduction of silica would be thorough with a sufficient Mg vapor. If the pressure of Mg vapor is not high enough, especially in the interfacial region of SiO_2 and MgO, Mg silicates such as Mg_2SiO_4 and $MgSiO_3$ may form as shown in **Figure 3D** via Eq. 5 and 6.

$$2MgO(s)SiO_2(s) \rightarrow Mg_2SiO_4(s) \quad (5)$$

$$MgO(s)SiO_2(s) \rightarrow MgSiO_3(s) \quad (6)$$

These reactions would consume the reactant SiO_2 and hence reduce the yield of Si. On the other hand, Mg silicates are detrimental to the electrochemical performance in batteries, which are not easy to remove thoroughly.

The Influence of Reaction Precursors

Specific micro-structure and morphology of SiO_2 can be maintained in the Si products which is one of the most important superiorities of MTR. The selection of precursor with special composition, structure and morphology could help to prepare various nano-structured Si materials. In general, there are several kinds of SiO_2 precursors, including the synthetic SiO_2 from TEOS (tetraethoxysilane) (Zhou et al., 2016; Chen et al., 2018b,c, 2019), biological origin silica (Liu et al., 2015; Sola-Rabada et al., 2018; Yu et al., 2018; Zhao et al., 2019), silica from sand (Ahn et al., 2017; Furquan et al., 2018), and natural clay minerals (Zhou et al., 2016; Chen et al., 2018b,c, 2019).

In 1968, W. Stöber (Stöber et al., 1968) proposed a controllable growth of spherical SiO_2 particles by hydrolysis of TEOS and the following condensation of silicic acid, as shown in **Figure 4A**. SiO_2 spheres from this facile and effective method present the uniform and controllable size, high chemical purity, and surface-functionality. The surface of SiO_2 synthesized *via* Stöber's method is decorated by the -OH groups, which is beneficial for structure stabilization and surface engineering with other coating layers. With the assistant of surfactant, hollow SiO_2 spheres can be obtained (Teng et al., 2012).

Therefore, SiO_2 synthesized by the Stöber method could act as an excellent precursor in MTR to achieve controllable structure and to investigate the mechanism of reaction. For example, based on the Stöber method, the porous 3-dimentional silica Santa Barbara Amorphous N. 15(SBA-15) and Mobil Composition of Matter N. 41 (MCM-41) can be prepared, and the porous structure can be sustained in the Si product after reduction.

As the essential element, Si exists widely in plants like husk of fruits and rootstock, playing an important role in their growth and healthy. Various biological materials, especially the agriculture waste, can be utilized as silica source in MTR (Rehman et al., 2019). For instance, in the rice husk, the element Si exists mainly in an amorphous or hybridization form. In general, silica of biological origins is environmentally friendly, cheaper, recyclable, and suitable for large-scale production. However, almost all the biologically originated silica materials contain carbon, which may form SiC during reduction where local temperature is quite high, and the content of SiC may worsen the electrochemical properties of Si, leading

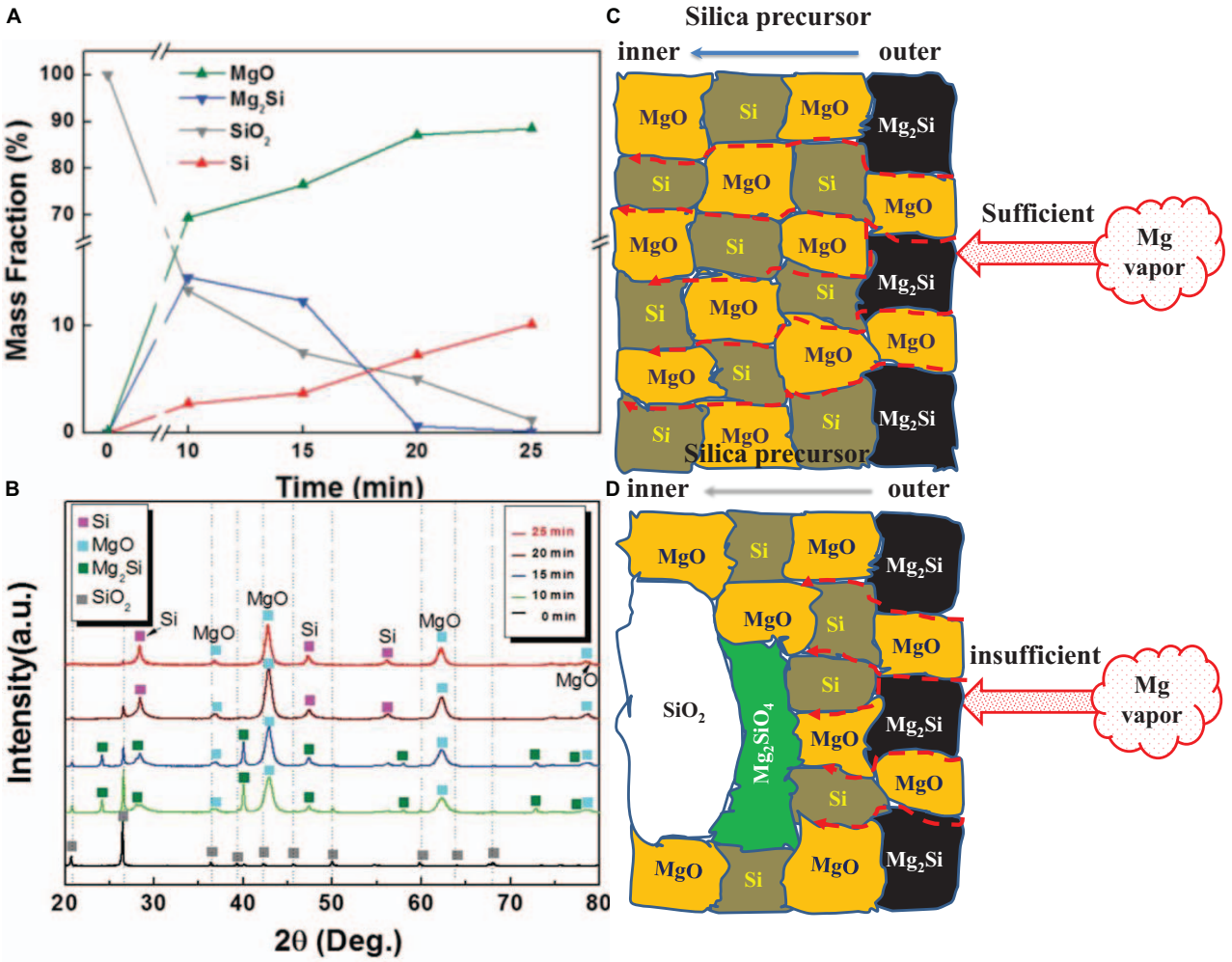

FIGURE 3 | XRD **(A)** and Changes in the product contents **(B)** with the reaction time, Reprinted from Ref. (Yoo et al., 2014), with the permission of John Wiley and Sons. **(C,D)** show the constitution of the products at different stages of the reduction process.

to capacity decay. Liu et al. (2013) prepared SiNPs from rice husk by acid leaching, annealing, and then MTR. The obtained uniquely small Si nanomaterial sustained the porous structure of rice husk as shown in **Figure 4B**, and exhibited good electrochemical performance in LIBs. Liu et al. (2015) fabricated a three-dimensional porous Si material from another biomass, the natural reed leaves, by calcination and MTR. As shown in **Figure 4C**, the lamella and porous structure in original reed leaves could be perfectly replicated in the final Si products.

Sand is one of the easiest obtainable precursors to be purified to high purity crystalline SiO_2. Favors et al. (2014) prepared porous nano-Si from beach sand. They formed an amorphous carbon coating on the nano-Si and achieved a remarkable cyclic capacity of 1,024 mAh g^{-1} at 2 A g^{-1} after 1,000 cycles. It should be mentioned that the reaction is in a low Si yield and the product is with a high mass fraction of Mg_2Si. This is because of the hindered Mg vapor diffusion in the dense and crystalline structure of sand derived SiO_2. The Mg vapor pressure would distribute higher in the outer part but lower in the inner part of the SiO_2.

On the other hand, SiO_2 from sand are always in a broader size distribution and irregular in morphology, resulting in the agglomeration in final Si products. Researchers (Ahn et al., 2017) reused the Mg_2Si in products to reduce SiO_2 for a higher reduction conversion rate. Besides, waste glass fibers, glass bottles have all been proved to be successful precursors in Si preparation (Li et al., 2017; Kang et al., 2020).

Natural clay minerals with various microstructures like tabular halloysite of lamella montmorillonite could also be used to produce Si in MTR. This kind of natural and low-cost Si sources could help to prepare nano-structured Si with the same specific structures as themselves. Bao et al. (2007) converted the intricate nanostructured silica of diatoms into continuous, nanocrystalline mixtures of Si and magnesia by MTR, as shown in **Figure 4D**. An interconnected network of Si nanocrystals was obtained after selective dissolution, which retained the 3-D frustule morphology of diatoms. Liu et al. (Sainan et al., 2018) prepared SiNPs by

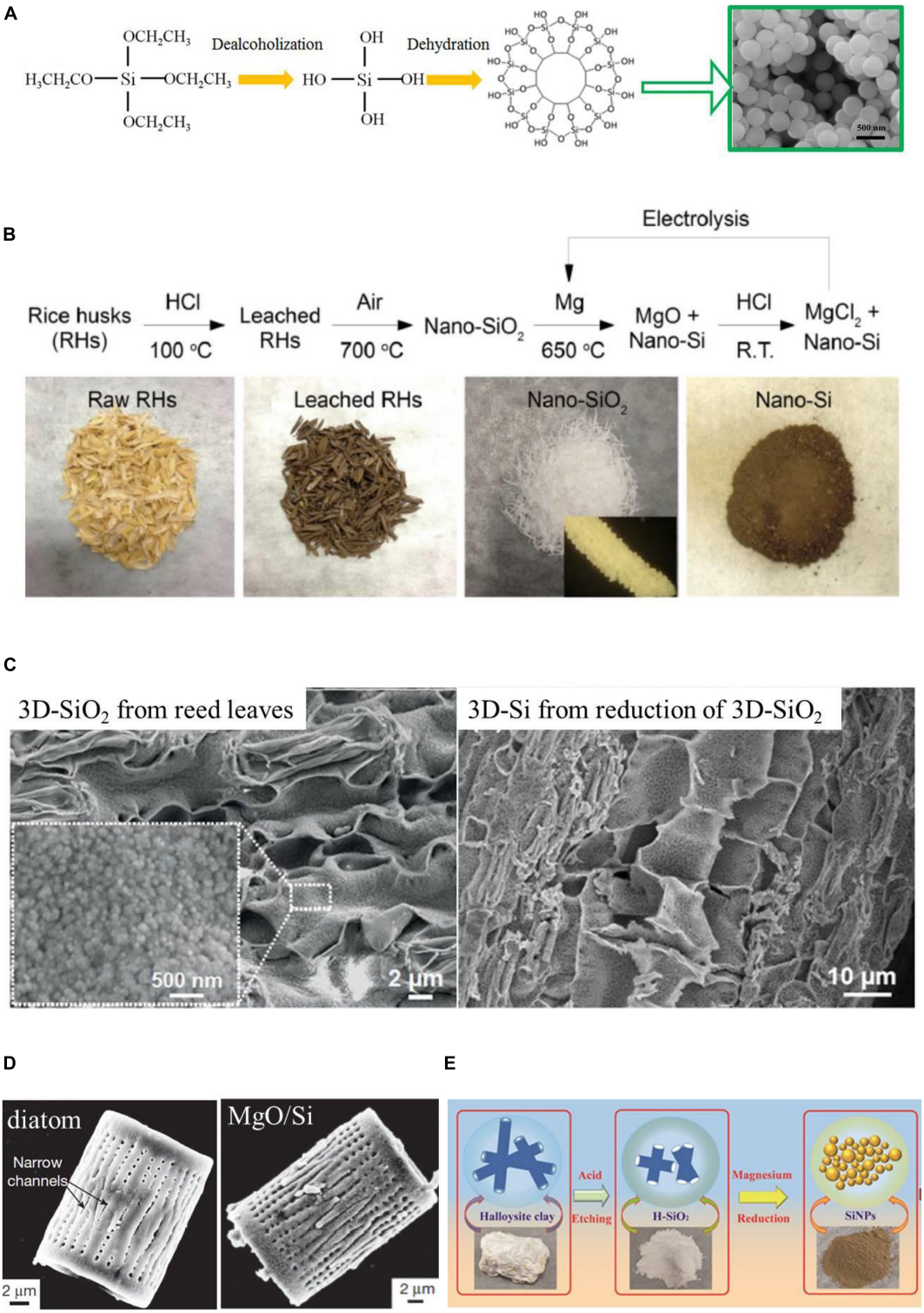

FIGURE 4 | (A) Schematic of TEOS hydrolyses and condenses to form silica and SEM images of the prepared SiO_2. **(B)** Flow chart of the process for recovering SiNPs from rice husk and the optical images of the intermediate substances. Reprinted from Ref. (Liu et al., 2013), with the permission of Springer Nature. **(C)** SEM image of highly porous and 3D hierarchical microstructures of SiO_2 from reed leaves and the received Si. Reprinted from Ref. (Liu et al., 2015), with the permission of John Wiley and Sons. **(D)** SEM images of diatom and the MgO/Si composition from reduction of diatom SiO_2. Reprinted from Ref. (Bao et al., 2007), with the permission of Springer Nature. **(E)** Schematic illustration of producing SiNPs from the halloysite preparation process. Reprinted from Ref. (Sainan et al., 2018), with the permission of MDPI.

the MTR of natural clay halloysite as illustrated in **Figure 4E**. They further combined the SiNPs with carbon fibers to prepare Si coated carbon fibers.

Analysis of Reaction by-Products

Size and morphology controllable Si nanomaterials are the target product in MTR. However, the existence of some inevitable by-products including MgO, Mg_2Si, $MgSiO_3$, Mg_2SiO_4 and unreacted Mg and SiO_2 would obviously reduce the yield of Si product (Entwistle et al., 2020).

MgO is the most dominant by-product, which distributes in the whole Si structure uniformly. It can be easily removed by the HCl treatment, leaving a porous Si structure that can accommodate the volume expansion during Li^+ ion insertion. Such a porous structure could also increase the interface area between Si and the electrolyte. The porous structure could provide a higher reversible capacity in terms of cycling and rate variation.

As discussed above, the by-product Mg_2Si would form at the very first stage and then react with SiO_2 in the following reaction stages. It mainly distributes in the surface region. Mg_2Si can also be removed by acid leaching, but the existence of Mg_2Si would reduce the yield of Si by consuming Si. While using a SiO_2 precursor with small sizes, the large specific surface area may lead to the formation of a large amount of Mg_2Si (Xie et al., 2014; Shi et al., 2016; Entwistle et al., 2018; Yang et al., 2020).

At low Mg vapor pressures and higher temperatures, Mg silicates ($MgSiO_4$ and Mg_2SiO_3) could form especially in the internal part of SiO_2 (Cordova and Shafirovich, 2020). The formation of Mg silicates is not with high probability and the concentration is usually low. Since these silicates have no or very low capacity contribution and may hinder the transportation of charge carriers, they are harmful to the electrochemical performance of the negatrode materials. The removal of silicates by mixed HCl and HF may release the toxic SiF_4. The silicate formation can be avoided at lower temperatures and optimized Mg vapor pressures. For instance, with a uniform temperature distribution and a higher Mg concentration in all parts of the SiO_2/MgO interface, no characteristic peak from silicates was detected by XRD of the Si product (Saeedifar et al., 2013; Xie et al., 2014; Yang et al., 2020).

As mentioned above, several different silica sources can be utilized in MTR. Silica from the biological origin and natural minerals always contain other elements like carbon and metallic impurities like Ca, Al, and transition metals (Aggrey et al., 2020b). Most of the metal oxides including CaO, Fe_2O_3, Al_2O_3, and Na_2O can be removed in the pre-leaching process.

As the most important and basic element in biomaterials, carbon exists widely and abundantly. It may react with SiO_2 and Mg via Eq. 7 at high temperature (1,400°C) (Zhang and Li, 2020).

$$SiO_2CMg \rightarrow MgOSiCSi \tag{7}$$

The effect of SiC on MTR products is complicated. On one hand, SiC presents good mechanical property and can help to form and maintain the structure of products both at reduction stage and in the lithiation/delithiation processes, leading to a stable electrode structure and good cyclic capacity. On the other hand, due to its poor electrochemical performance, the content of SiC in the active material may result in lower conductivity and low capacity (Li et al., 2016).

Al_2O_3 in the natural clay could also react with Mg as the following reactions, which may consume the reductant Mg and reduce the Si yield (Chen et al., 2018c).

$$Al_2O_3Mg \rightarrow AlMgO \tag{8}$$

$$AlSiO_2 \rightarrow Al_2O_3Si \tag{9}$$

In some cases, the generated Al may reduce SiO2 again according to reaction (9).

The Influence of Reaction Conditions

Generally, the MTR is carried out at a temperature which is a little higher than melting point of Mg under the atmosphere of mixed Ar and H_2 (95:5 in volume) or vacuum. A series of reaction parameters play important roles in the reduction process, including temperature, time, ratio of Mg/SiO_2, reactor type, and the use of a heat scavenger. In this section, influences of several reaction conditions are discussed according to abundant research results and deduce the applicable parameters in MTR for a preferable Si product both in yield and structure.

Influence of Heat Scavenger

As mentioned in 2.1, MTR is a highly exothermic reaction. The temperature at local regions may reach a very high level (the max point may be 1,941°C), leading to collapse of the porous structure constructed by reduction and aggregation of Si nanomaterials (Won et al., 2011). Besides, the high temperature may promote some side-reactions, including the formation of Mg_2Si and Mg silicates under different Mg vapor pressures, and of SiC in the presence of carbon.

Some heat scavengers including NaCl, KCl, and KI, have been used to absorb the released heat to avoid self-fusion by covering around SiO_2 particles. Favors et al. (2014) added NaCl into the MTR process and synthesized an interconnected 3D network of nano-Si from beach sand. As the most conventional heat scavenger, NaCl is low cost, non-toxic, highly conducting to heat (0.8 W m^{-1} K^{-1}) (Galamba et al., 2004), and easy to recycle. Furthermore, there is no other reactions involved during the reduction of SiO_2. The melting enthalpy of NaCl is 28.8 KJ mol^{-1}. The emitting heat from the reaction between Mg and SiO_2 can firstly cause the fusion of NaCl, instead of Si or SiO_2, at 801°C which is the melting point of NaCl.

The addition of heat scavengers could promote a more uniform reaction in different regions, helping to sustain the morphology, especially the porous and dispersive structures of Si. Heat scavengers could also improve the Si yield by suppressing side-reactions. Moreover, the heat scavenger can make the reaction more controllable and further help scaling-up of this method.

In addition to NaCl (Wang et al., 2017; Aggrey et al., 2020a,b; Li Y. et al., 2020), KCl (Liu et al., 2016) (T_m = 770°C), and KI (Han et al., 2019) (T_m = 681°C) could also be selected to absorb

heat in MTR. Among these four compounds, KI is most sensitive, since its melting point is closest to the reduction temperature (Han et al., 2019). Therefore, KI could control the temperature in reaction more precisely and help to reduce the amount of SiC in products for a higher Si yield. $MgCl_2$ (Cordova and Shafirovich, 2020) and $AlCl_3$ (Lin et al., 2020) can also be used as heat absorption agents.

Mass Ratio of Mg/SiO_x

According to reaction (2) for MTR, the stoichiometric ratio of Mg and SiO_2 should be 2 to 1 in mole. As discussed in see section "Reaction Mechanism and Process" on the reaction mechanism, the Mg vapor pressure controls the reduction process and influences the reaction products. Mg reacts as a vapor and is prone to escape with the Ar/H_2 gas flow. Therefore, the ratio of Mg/SiO_2 should be equal to or a little higher than 2. Barati et al. (2011) investigated the product compositions by XRD with different ratios of Mg/SiO_2 and findings can be seen in **Figure 5A**. By comparing the relative heights of specific peaks, it is suggested that the contents of Si, MgO, SiO_2, and Mg_2Si are strongly affected by the ratio of Mg/SiO_2. At a low ratio, the Mg vapor is not adequate to reduce all the silica, but when the Mg vapor pressure is too high, the formation of Mg_2Si becomes more remarkable. The ratio around 2 promoted the highest Si yield. A similar effect has been proven by calculation in 2017 (Zakaryan et al., 2017), as shown in **Figure 5B**. A ratio of near 2 would lead to complete reduction. Lower and higher ratios would lead to by-products like Mg_2Si as a result of an insufficient or excessive supply of the Mg vapor.

One advantage of MTR is the controllable microstructure and porous morphology. The Mg/SiO_2 ratio also influences the size and pore size of the Si product. According to Entwistle et al. (2020), as the Mg/SiO_2 ratio increases, the pore size increases and becomes sustained while the ratio is between 2.0 and 2.5. The crystal size remains nearly the same at various ratios.

Temperature and Time (Phase Transition of Products Under Different Time Gradients and Reaction Temperature Gradients)

Generally, the reaction temperature of MTR is set to be slightly higher than 648°C which is the melting point of Mg. In that case, Mg is liquid in the form of droplets dispersed in the SiO_2 matrix. Also these droplets can also react with SiO_2, it is the vapor of the droplets that can diffuse quickly through the porous SiO_2 matrix and reduce the latter with a better contact and higher reaction efficiency. Meanwhile, because MTR highly exothermic, the temperature at and near the reaction sites may go up once the reduction starts. For this reason, the set temperature should not be too high in order to prevent side reactions and particle agglomeration. Therefore, the temperature and temperature gradients during the reaction can exert two important effects: the purity, and the porous structure and morphology of the products.

Investigations on effects of reaction temperatures can be seen in **Figures 6A,B**. From 550 to 950°C (Entwistle et al., 2020), the average crystal size increases and the pore size increases as a result of high temperature sintering. The larger pore size would result in higher specific surface area which is a key parameter for electrochemical performance of Si. At higher temperatures, the purity of Si increases because Mg_2Si can reduce SiO_2 more thoroughly, and the diffusion of the Mg vapor is faster and more effective. As a result, considering both purity and morphology, a moderate temperature should be applied in order to achieve a high yield of Si nanomaterial with a controllable microstructure.

As mentioned in see section "Reaction Mechanism and Process," the Mg vapor would react according to Eqs. 2 and 3 and Mg_2Si is formed at the starting stage of the reduction and could further reduce SiO_2 to Si in the following stages. Therefore, the reduction is becoming more complete and the purity of Si also increases with a longer reaction time. If the reaction time is not long enough under low temperatures, the diffusion of Mg may be insufficient and usually Mg_2Si can be detected. Longer reaction time can lead to the lower amount of Mg_2Si. However, excessive reaction time may result in the exhaustion of Mg, leading to the formation of MgO and Mg silicates, as well as the sintering of both MgO and silicon (Waitzinger et al., 2015; Yan and Guo, 2019; Guo et al., 2020).

Reactor

The Mg vapor diffusion to the reaction interface between the vapor and silica controls the whole reaction process. Rational design of the MTR reactor could obtain a preferable Mg vapor distribution. There are mainly two types: sealed and open reactors. Sealed reactors could further be divided into the up-down type and disconnect type according to the way of contacting between the Mg powder and SiO_2 precursor. The schematic diagrams of these three types can be seen in **Figure 7**, in which the red line presents the flow direction of the Mg vapor. The open reactor (**Figure 7A**) is a boat filled with the uniform mixture of Mg, SiO_2 and NaCl prepared by intensive stirring and grinding. The furnace is filled with mixed Ar and H_2 gasses. The uniform mixing ensures good contacts and sufficiently large interfaces between the Mg and SiO_2 particles. This method is simple, reproducible, and most widely used, but the local temperature inside of the powder is always higher than outside, which in turn leads to the Mg vapor pressure being higher inside than outside. This is because that the Mg vapor will be taken away by Ar/H_2 gas Thus, the color of the product changes from inside to outside, indicating the content difference in the products.

Figure 7B (Xie et al., 2014; Wissel et al., 2017) shows the structure of the up-down sealed reactor, which is separated by a stainless steel plate with three holes. The SiO_2 powder is loaded on the plate while the Mg powder is underneath. Then the apparatus is sealed in Ar-filled glove box, and then placed into the tube furnace. During the thermal treatment, Mg converts into vapor and diffuses up to the surface of the SiO_2 powder. In **Figure 7C**, the reactor is also sealed with an inert gas, but Mg and SiO_2 powders are placed in two adjacent boats (Tao et al., 2012). Compared with the open reactor in **Figure 7A**, the two the sealed reactors in **Figures 7B,C** enable better utilization of the Mg reductant and the Mg vapor pressure can be controlled more adequately, leading to a higher Si yield. However, the sealed reactors may increase the cost and the difficulty for mass production.

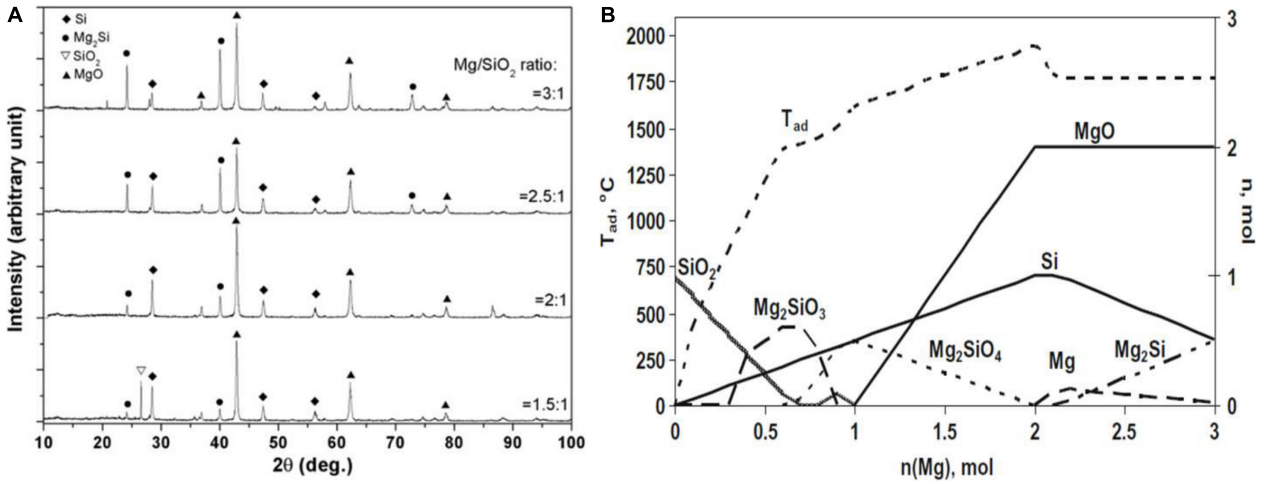

FIGURE 5 | (A) XRD patterns of products from reactions between SiO_2 and Mg at different ratios. Reprinted from Ref. (Barati et al., 2011), with the permission of Elsevier. **(B)** Calculated influences of Mg powder usage and temperature on product composition by simulation. Reprinted from Ref. (Zakaryan et al., 2017), with the permission of Springer Nature.

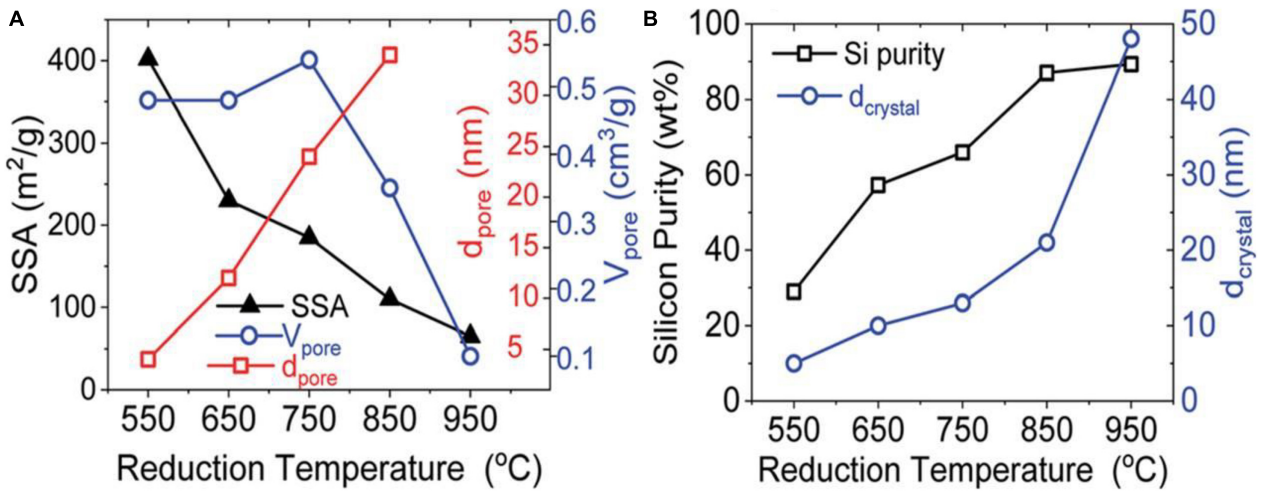

FIGURE 6 | The influence of the **(A)** average pore diameter (d_{pore}), specific surface area (SSA), and pore volume (V_{pore}), and **(B)** the average pore diameter ($d_{crystal}$) and silicon purity under the reaction at different temperatures. Reprinted from Ref. (Entwistle et al., 2020), with the permission of Royal Society of Chemistry.

INTERFACE CONTROL OF SILICON DERIVED FROM MAGNESIOTHERMIC REDUCTION AND ITS APPLICATION IN LIBS

Silicon nanomaterials prepared by MTR have advantages of porous, sustained and controllable morphology, and high purity after acid leaching. The porous micro-structure could bring about better tolerance to volume change during lithiation and delithiation. It also enlarges the specific surface area which is beneficial to carrier transportation. However, problems of fracturing and contact loss caused by large volume expansion could not be solved. Especially when the size is larger than 150 nm, and the repeating SEI may form and exhaust Li^+ ion, resulting in an unstable Si/electrolyte interface. Many efforts have been made on the surface and interface modification for Si negatrodes derived from MTR, after or before the reduction. These modifications have improved the electrochemical performances in LIBs significantly. **Supplementary Table 1** compares various Si materials prepared from different precursors via MTR, as well as their performance parameters in LIBs.

Interface Modification on the Reduced Silicon From Magnesiothermic Reduction

Many surface and interface modification strategies for Si electrode materials have been developed, including incorporation of carbon, oxides, and composite shells outside of Si. The most

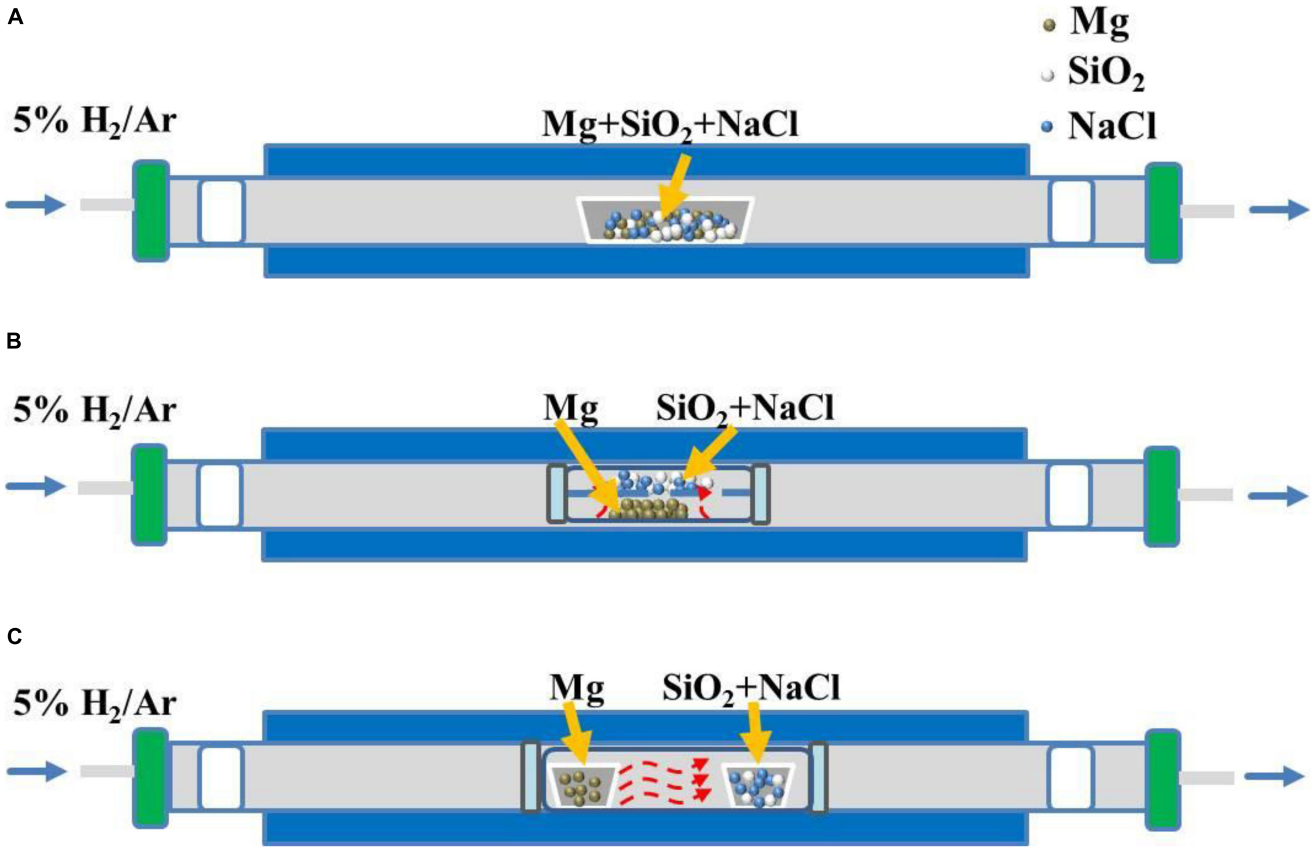

FIGURE 7 | (A) Commonly used direct mixing reactor, **(B)** Magnesium vapor diffuses from bottom to top in a closed reactor, **(C)** Horizontal diffusion of magnesium vapor in a closed reactor.

commonly used Si modification is carbon coating, which could composite with Si derived from different precursors to achieve better electrochemical performance.

The most primary Si nanomaterials are the monodispersed spheres prepared via the Stöber MTR route. Xie et al. (2014) prepared SiNPs using 400 nm SiO_2 particles as the precursor and then coated the SiNPs with a carbon layer of various thickness by the CVD method (**Figure 8A**). The amorphous carbon could buffer the volume change and improve the electron and Li^+ ion transport, achieving a higher capacity of 800 mAh g^{-1} for the Si/C composite compared to 200 mAh g^{-1} for the bare Si after 50 cycles.

Zhang et al. (2016) prepared the Si/N-doped carbon/CNTs composite sphere by MTR using rice husk as the Si source and then performed carbon coating by an electrospray method. As shown in **Figure 8B**, the micro/nano hierarchical hybrid sphere with a diameter of 3 to 4 μm consists of SiNPs derived from rice husk. The SiNPs were wrapped with CNTs in the N-doped carbon matrix. The hybrid hierarchical structure could provide more space and strength for the volume expansion of Si. The carbon coating could improve electron conduction during the dis-/charging processes. After 100 cycles, the reversible capacity was as high as 1,031 mAh g^{-1}.

The aforementioned SiNPs reduced from beach sand by Favors et al. (2014) were then coated with carbon by pyrolysis of C_2H_2. It can be seen in **Figure 8C** that the Si/C composites exhibited the preferable capacity of 1,000 mAh g^{-1} after 1,000 cycles at 2 A g^{-1}. Ahn et al. (2017) also conducted MTR on sea-sand and then prepared Si/C composites with various carbon/Si ratios. After carbon coating, higher cyclic capacity was achieved due to the improved structural stability.

Diatomite, a natural mineral, can be reduced to Si and further converted to a porous structure after rinsing in acid to remove metal oxides. Tang et al. (2018) coated carbon on the porous Si with dopamine hydrochloride in solution and received the composites (**Figure 8D**). This porous Si/C composites showed high capacity of 1,227 mAh g^{-1} at 2 A g^{-1}.

Generally, carbon coating is one of the most significant interface modification methods for Si negatrode application in LIBs, not only for Si prepared by MTR but also by other methods. The good mechanical strength of carbon could buffer the volume change of Si during the dis-/charging process, resulting in a more stable structure. The carrier transport efficiency of the whole active material could be improved because of the good electron and Li^+ ion conductivity. However, this strategy always needs two or more steps, leading to a more complicated process and is difficult for mass production. The advantages of MTR prepared

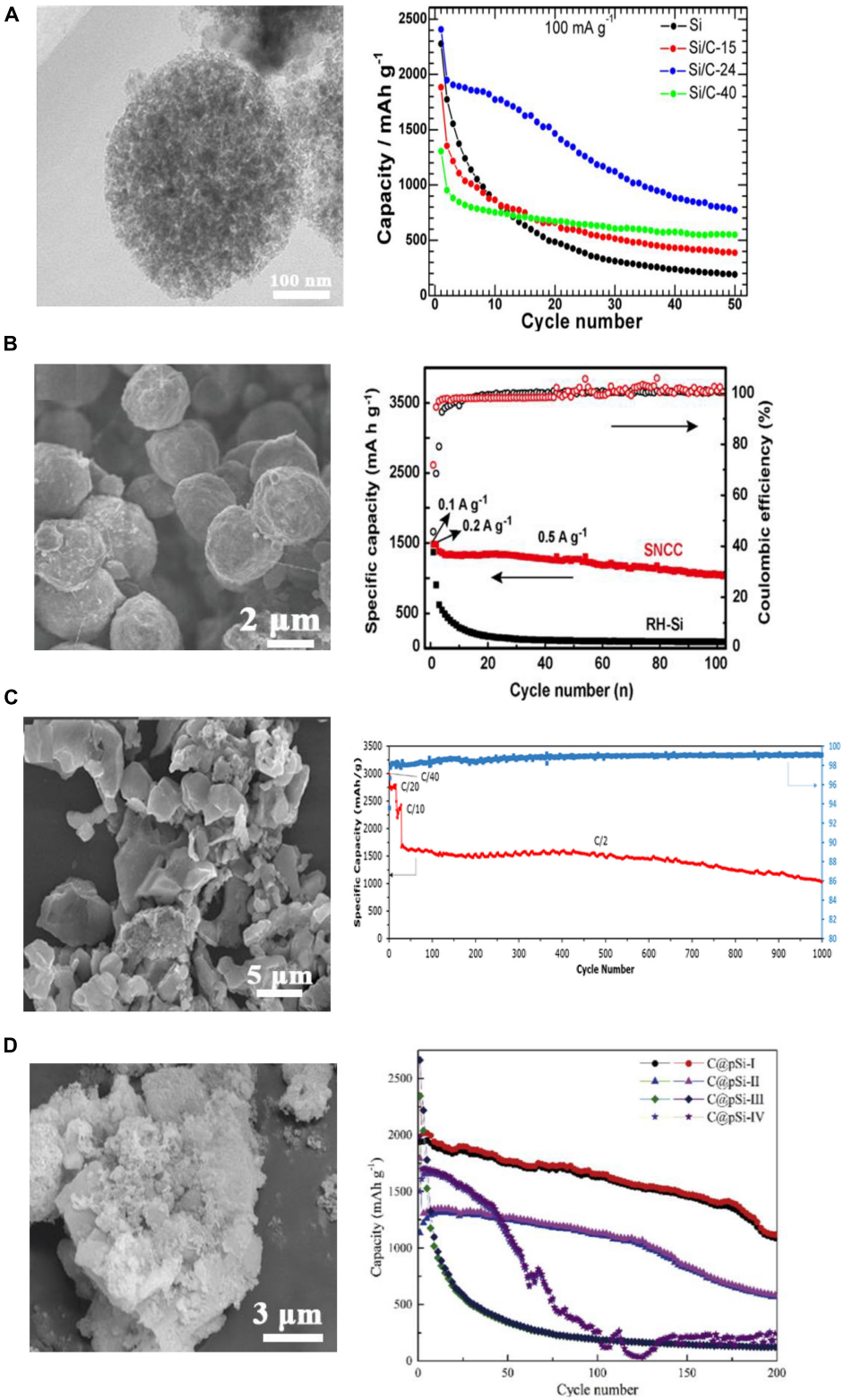

FIGURE 8 | SEM image and cycling performance of **(A)** Si/C spheres, reprinted from Ref. (Xie et al., 2014), with the permission of Elsevier. **(B)** Si/C derived from rice husk, reprinted from Ref. (Zhang et al., 2016), with the permission of Elsevier. **(C)** porous Si@C from sand precursor, reprinted from Ref. (Favors et al., 2014), with the permission of Scientific Reports. **(D)** porous Si@C derived from clay. Reprinted from Ref. (Tang et al., 2018), with the permission of Elsevier.

Si in morphology and structure may be compromised during the following coating step.

Surface Modification on Synthetic Silica for Magnesiothermic Reduction

Magnesiothermic reduction could help construct a high specific surface area of Si that can support a higher ionic carrier mobility. In order to prepare stable Si nanomaterials with controllable size and morphology, the reaction parameters should be elaborated, designed and confirmed. The temperature, temperature changing rate, precursor mixing, atmosphere, and time can all influence the reduction process. For a reproducible MTR, the stability of the SiO_2 precursor is also important. Many efforts have been made on interface modification of the synthetic silica, including carbon coating and metal oxides combination.

Using carbon coated silica as precursors, Si/C composites could be directly received by one-step MTR. Zhu et al. (2017) synthesized SiO_2 sphere by Stöber method, and further mixed with graphene oxide to obtain SiO_2/GO composites. The composites were then undergone the MTR to Si/G composites (GO: graphene oxide; G: graphene from reducing graphene oxide). A better stability of the hybrid material can be achieved by combining with graphene, and the micro-structure could remain integrated. The Si/G composites presented a lower initial capacity but a higher retention during cycling, which can be seen in **Figure 9A**. Similar results were obtained by Wu et al. (2016) They deposited SiO_2 directly on the graphene oxide nanosheets by hydrolysis of TEOS. 3D Si@G composites could be obtained with excellent electrochemical performance after MRT.

Difunctional methacrylate monomers were used as a carbon matrix for SiO_2 spheres from the Stöber method in 2019 (Zuo et al., 2019). The 3D Si/C composites were obtained by MTR and exhibited 710 mAh g^{-1} after 300 cycles. In addition, the hydrolysis of TEOS on CNTs could form the SiO_2/CNTs hybrid which was then converted to the Si/CNTs composites via MTR (**Figure 9B**; Zhang et al., 2019). The bonding between SiO_2 and CNTs could help SiO_2 anchoring on the CNTs network, improving the electron conduction, and therefore an improved electrochemical property could be achieved.

Generally, caron coating is always stable during the MTR process, which could make the morphology of composite more sustainable and promote the long cycle and high rate performance of Si/C composites. Sometimes, carbon coating could be beneficial to constructing other new morphology of composites, like the yolk-shell Si@void@C material (Li X. et al., 2020). Nevertheless, the existence of carbon in MTR may cause the formation of SiC under certain conditions. As mentioned in see section "Reaction Mechanism of the Magnesiothermic Reduction of Silica," SiC could maintain the matrix structure of the hybrid material, but it could also be detrimental to the total properties due to its poor electrochemical performance.

Metal oxides like TiO_2 could act as a coating material of SiO_2 to modify the surface of SiO_2. Kim Y.M. et al. (2015) prepared SiO_2@TiO_2 core-shell structured spheres followed by MTR and received the Si@$TiSi_2$ spheres, which are shown in **Figure 9C**. The $TiSi_2$ coating layer could improve the conductivity and structure stability during dis-/charging due to its good electrical conductivity and physical strength. Therefore, improved cycle and rate performance of Si composite in LIBs can be received. In 2017, (Jia et al., 2017), a sandwich-structured C/Si/TiO_x nanofiber composite was prepared through MTR of SiO_2/TiO_2 on carbon fibers. After 160 cycles, the reversible capacity retained at 793 mAh g^{-1} at 0.1 A g^{-1}. The TiO_2 coating layer on SiO_2 could transfer into TiO_x or $TiSi_2$ during the reduction process, and the excellent structural stability could enhance the strength of the composite by preventing the cracking of Si. TiO_x also provides some Li^+ ion insertion/de-insertion capacity. The synergistic effect of metal oxide and Si could stabilize the structure and carrier transport channel.

Morphology Control by Template-Assistance in Synthesis of Silica

Design and construction of special morphology, especially that with a higher specific surface area and larger space for Si expansion, are the commonly used and important strategy for surface modification of Si. There are quite a few investigations on the template-assisted synthesis of silica with special morphology like hollow or ordered porous structures. The surfactant control and metal oxide/metal organic frame assistance are the two widely used methods.

Comparing with the solid silica like sand or spheres, higher Si yield could be obtained with porous, especially the ordered porous silica due to the more efficient contact with Mg vapor. SiO_2 from TEOS hydrolysis could self-assemble into porous structure when some polymer agent is added as surfactant. This porous structure has larger specific surface area, and can be reduced by Mg into orderly and uniform pours structured Si. SBA-15, and MCM-41 are typical examples of the synthetic porous silica with specific porous structures. These ordered mesoporous silica could then be reduced into mesoporous Si, as can be seen in **Figure 10A**. After coating with carbon, the porous Si presented 1,800 mAh g^{-1} reversible capacity after 100 cycles (Li et al., 2015). MCM-41 is the silica source with a similar structure fabricated with the aid of a polymeric surfactant. It can be reduced by Mg and keep the initial morphology. As shown in **Figure 10B**, Shivaraju et al. (2019) prepared nano-porous nano-Si from MCM-41 through MTR. The highly porous Si demonstrated good cycling stability (705 mAh g^{-1} at 0.5°C after 500 cycles) and rate performance.

The template-assisted method has been applied to prepare a series of hollow structured Si via reducing the hollow structured silica. The sacrificial templates, including metal oxides and solid polymers, could act as sites of heterogeneous nucleation during the formation of silica and then be removed by etching in solution or heating. Therefore, the hollow structured silica with the same shape of the template can be received and undergo the following MTR.

As shown in **Figure 10C**, Wang et al. (2018) prepared ZnO@SiO_2 structure using ZIF-8 as template, and then removed ZnO by HCl leaching, leaving the hollow cubes of SiO_2. After the MTR and the following carbon coating process, a hollow

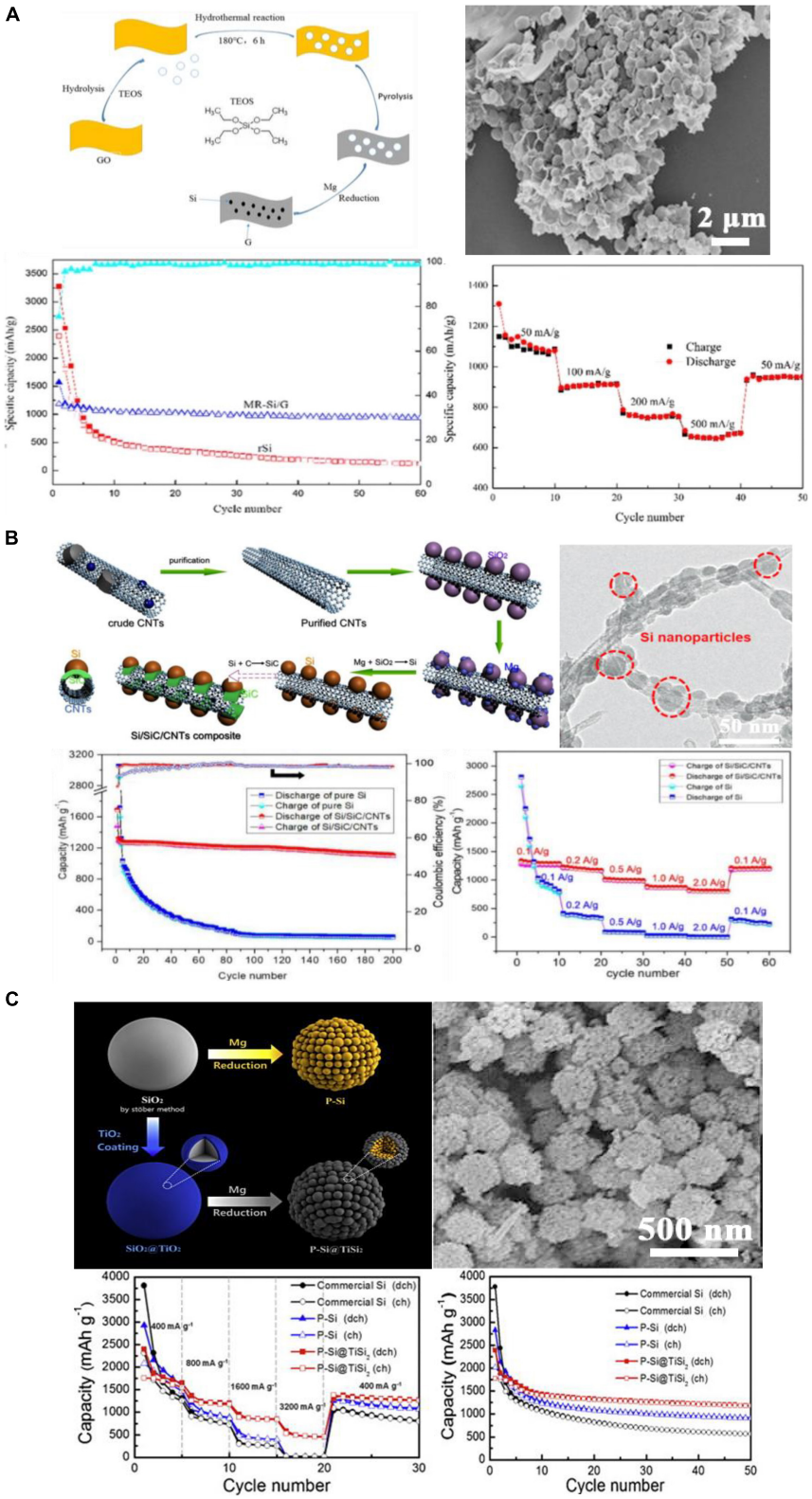

FIGURE 9 | (A) Schematic diagram of preparation, SEM, cycling and rate performance of Si/G reduced from SiO_2/GO. Reprinted from Ref. (Zhu et al., 2017), with the permission of Springer Nature. **(B)** Fabrication schematic diagram, TEM and electrochemical performance Si/CNTs reduced from SiO_2/CNTs. Reprinted from Ref. (Zhang et al., 2019), with the permission of MDPI. **(C)** Schematic, SEM, and rate performance of Si/$TiSi_2$ spheres. Reprinted from Ref. (Kim Y.M. et al., 2015), with the permission of Elsevier.

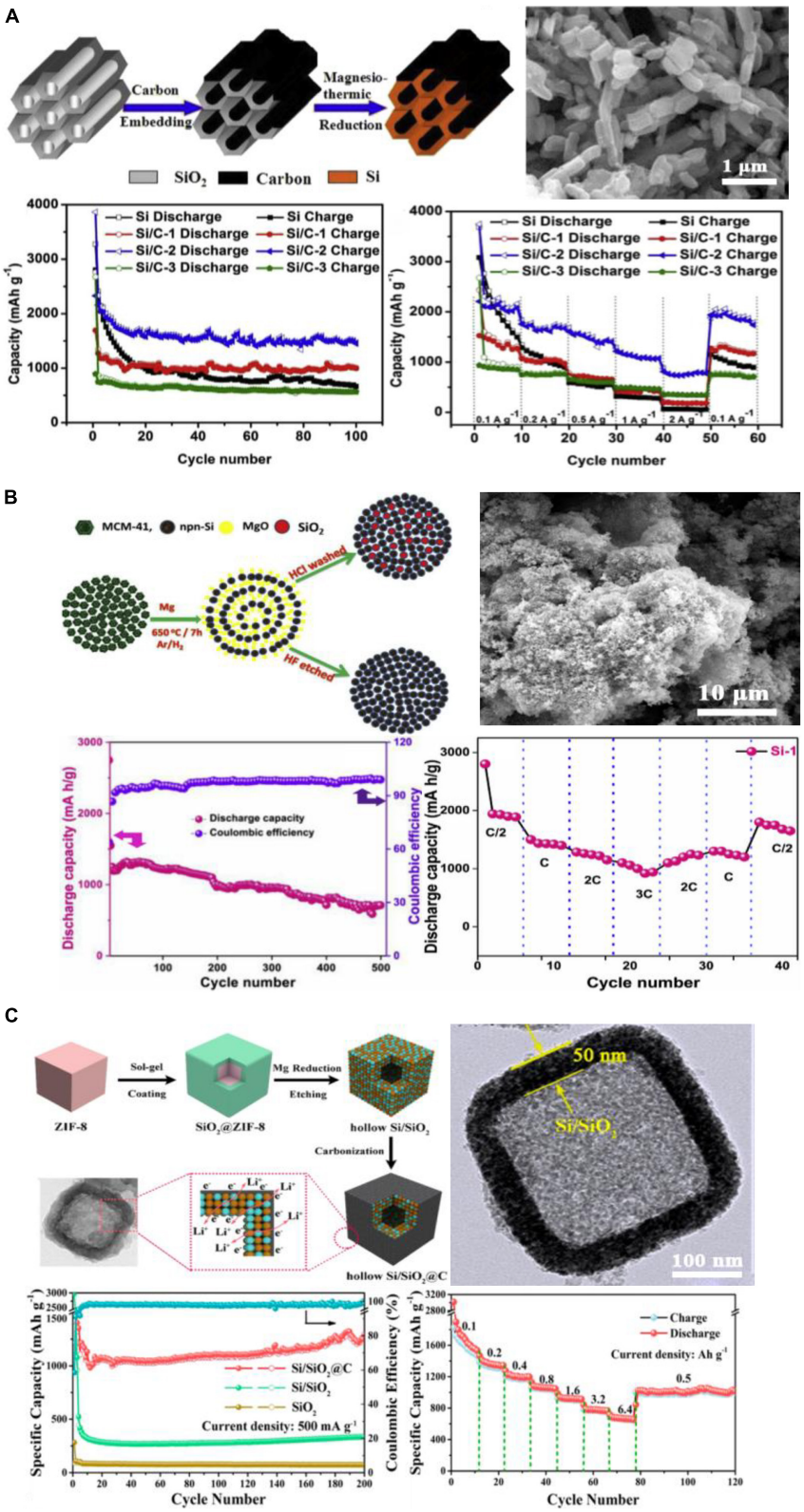

FIGURE 10 | (A) Fabrication, SEM, and electrochemical performance of ordered porous Si from SBA-15. Reprinted from Ref. (Li et al., 2015), with the permission of Elsevier. **(B)** Fabrication, SEM, cycle and rate performance of porous Si from reduction of MCM-41. Reprinted from Ref. (Shivaraju et al., 2019), with the permission of Elsevier. **(C)** Fabrication, TEM, and electrochemical performance of hollow Si/SiO_2@C using sacrificial template. Reprinted from Ref. (Wang et al., 2018), with the permission of American Chemical Society.

Si/SiO_2@C composite was received. Better stability was achieved during the large change in volume. The reversible capacity was as high as 1,250 mAh g^{-1} at 0.5 A g^{-1} after 200 cycles, and there was still a capacity of 667 mAh g^{-1} at a large specific current of 6.4 A g^{-1}.

In 2017, Ashuri et al. (2016b) prepared hollow Si nanospheres encapsulated with a carbon shell. The sacrificial polystyrene (PS) nanospheres could provide the nucleation surface for SiO_2 growth and then it was removed by step-wise programmed heating. The SiO_2 hollow spheres were then reduced by MTR and coated with carbon. Improved electrochemical results were achieved due to the special hollow structure of the HSi@C composite and the synergistic effects of the engineered void and conductive carbon shell.

CONCLUSION AND PROSPECTION

Because of the pursue of higher capacity and dis-/charging rates, the application of Si in LIBs has been proven to be effective with promising prospective applications. However, there is no consensus on fabrication methods and strategies to solve the remaining intrinsic problems of Si materials. Magnesiothermic reduction (MTR) is a promising way to the fabrication of porous Si with the advantages of low cost, simple and convenient process, and controllable morphology according to the precursor, and prone for interface modification. In this mini review, the thermodynamics and mechanisms of the reaction are reviewed and discussed, including the influences of the precursor and reaction conditions on the dynamics of the reduction. Mg_2Si may form at both the initial stage of the reduction and at high pressure of the Mg vapor, which may further reduce SiO_2 at the interface of SiO_2/Mg_2Si. If the Mg vapor is insufficient, the formation of Mg silicates is inevitable, leading to a low Si yield. The exothermic reduction process must be designed with the addition of heat scavenges, the temperature schedule, and the reactor optimisation. Also, the electrochemical performance of MTR produced Si as the negatrode of LIBs, and the surface modification and its effect on the performance have been analyzed summarized. Surface modification could maintain the porous structure derived from MTR, stabilize the morphology during dis-/charging processes, and improve the carrier transport efficiency by constructing a higher specific surface area and introducing highly conductive materials.

Up to now, there are still some obstacles limiting the mass production of Si by MTR, including the not high-enough Si yield, and the side reactions during the reduction. To realize commercial application, the precise control of the conditions in the MTR is decisive to achieve the desired specific surface area, porous structure, and stability of the Si product, which may influence the final electrochemical performance.

In addition to being used as the negatrode material in LIBs, porous Si *via* MTR can also be applied in photoluminescence, photocatalysis, drug delivery and as the carrier for other nanomaterials. The thorough comprehension on MTR would help better design the reaction process and achieve the desired Si properties.

AUTHOR CONTRIBUTIONS

TJ supervised the research project relevant to this article. GC and TJ discussed about, and agreed on TJ's proposal of the topic and outline of this review article. YT selected and summarized the relevant literatures and together with TJ prepared the manuscript. GC revised the manuscript in terms of scientific clarity and language. All authors discussed, reviewed, and commented on the manuscript.

FUNDING

This work was supported by the National Natural Science Foundation of China (No. 51602234).

SUPPLEMENTARY MATERIAL

The Supplementary Material for this article can be found online at: https://www.frontiersin.org/articles/10.3389/fenrg.2021.651386/full#supplementary-material

REFERENCES

Aggrey, P., Abdusatorov, B., Kan, Y., Salimon, I. A., Lipovskikh, S. A., Luchkin, S., et al. (2020a). In situ formation of nanoporous silicon on a silicon wafer via the magnesiothermic reduction reaction (MRR) of diatomaceous earth. *Nanomaterials (Basel)* 10:601. doi: 10.3390/nano10040601

Aggrey, P., Salimon, A. I., Abdusatorov, B., Fedotov, S. S., and Korsunsky, A. M. (2020b). The structure and phase composition of nano-silicon as a function of calcination conditions of diatomaceous earth. *Mater. Today: Proc.* 33, 1884–1892. doi: 10.1016/j.matpr.2020.05.358

Ahn, J., Lee, D.-H., Kang, M. S., Lee, K.-J., Lee, J.-K., Sung, Y.-E., et al. (2017). Sea sand-derived magnesium silicide as a reactive precursor for silicon-based composite electrodes of lithium-ion battery. *Electrochim. Acta* 245, 893–901. doi: 10.1016/j.electacta.2017.05.164

Ashuri, M., He, Q., and Shaw, L. L. (2016a). Silicon as a potential anode material for Li-ion batteries: where size, geometry and structure matter. *Nanoscale* 8, 74–103. doi: 10.1039/c5nr05116a

Ashuri, M., He, Q., Zhang, K., Emani, S., and Shaw, L. L. (2016b). Synthesis of hollow silicon nanospheres encapsulated with a carbon shell through sol–gel coating of polystyrene nanoparticles. *J. Sol-Gel Sci. Technol.* 82, 201–213. doi: 10.1007/s10971-016-4265-z

Ba, J., Li, H., Lin, J., Ren, B., Zheng, X., Qi, J., et al. (2019). Magnesiothermic reduction of SiO2f/SiO2 composites for brazing with Nb using AgCuTi. *J. Manuf. Process.* 46, 26–33. doi: 10.1016/j.jmapro.2019.08.024

Bao, Z., Weatherspoon, M. R., Shian, S., Cai, Y., Graham, P. D., Allan, S. M., et al. (2007). Chemical reduction of three-dimensional silica micro-assemblies into microporous silicon replicas. *Nature* 446, 172–175. doi: 10.1038/nature05570

Barati, M., Sarder, S., McLean, A., and Roy, R. (2011). Recovery of silicon from silica fume. *J. Non-Cryst. Solids* 357, 18–23. doi: 10.1016/j.jnoncrysol.2010.09.079

Buqa, H., Holzapfel, M., Krumeich, F., Veit, C., and Novák, P. (2006). Study of styrene butadiene rubber and sodium methyl cellulose as binder for negative electrodes in lithium-ion batteries. *J. Power Sources* 161, 617–622. doi: 10.1016/j.jpowsour.2006.03.073

Cai, H., Han, K., Jiang, H., Wang, J., and Liu, H. (2017). Self-standing silicon-carbon nanotube/graphene by a scalable in situ approach from low-cost Al-Si alloy powder for lithium ion batteries. *J. Phys. Chem. Solids* 109, 9–17. doi: 10.1016/j.jpcs.2017.05.009

Chen, Q., Liu, S., Zhu, R., Wu, D., Fu, H., Zhu, J., et al. (2018b). Clay minerals derived nanostructured silicon with various morphology: controlled synthesis, structural evolution, and enhanced lithium storage properties. *J. Power Sources* 405, 61–69. doi: 10.1016/j.jpowsour.2018.10.031

Chen, Q., Zhu, R., Deng, L., Ma, L., He, Q., Du, J., et al. (2019). One-pot synthesis of novel hierarchically porous and hydrophobic Si/SiOx composite from natural palygorskite for benzene adsorption. *Chem. Eng. J.* 378:122131. doi: 10.1016/j.cej.2019.122131

Chen, Q., Zhu, R., Fu, H., Ma, L., Zhu, J., He, H., et al. (2018c). From natural clay minerals to porous silicon nanoparticles. *Microporous Mesoporous Mater.* 260, 76–83. doi: 10.1016/j.micromeso.2017.10.033

Chen, Q., Zhu, R., Liu, S., Wu, D., Fu, H., Zhu, J., et al. (2018a). Self-templating synthesis of silicon nanorods from natural sepiolite for high-performance lithium-ion battery anodes. *J. Mater. Chem. A* 6, 6356–6362.

Chen, Y., Du, N., Zhang, H., and Yang, D. (2015). Facile synthesis of uniform MWCNT@Si nanocomposites as high-performance anode materials for lithium-ion batteries. *J. Alloys Compd.* 622, 966–972. doi: 10.1016/j.jallcom.2014.11.032

Chen, Y., Qin, Y., Lu, B., Yang, H., Qin, Y., Li, F., et al. (2017). Large-scale production of silicon nanoparticles@graphene embedded in nanotubes as ultra-robust battery anodes. *J. Mater. Chem. A* 5, 4809–4817.

Cho, J. H., and Picraux, S. T. (2014). Silicon nanowire degradation and stabilization during lithium cycling by SEI layer formation. *Nano Lett.* 14, 3088–3095. doi: 10.1021/nl500130e

Cordova, S., and Shafirovich, E. (2020). Combustion synthesis of nanocrystalline silicon from silica and magnesium silicide. *Mater. Chem. Phys.* 254:123288. doi: 10.1016/j.matchemphys.2020.123288

Ellingham, H. J. T. (1944). Reducibility of oxides and sulfides in metallurgical processes. *J. Soc. Chem. Ind.* 63, 125–133.

Entwistle, J., Rennie, A., and Patwardhan, S. (2018). A review of magnesiothermic reduction of silica to porous silicon for lithium-ion battery applications and beyond. *Journal of Materials Chemistry A* 6, 18344–18356. doi: 10.1039/c8ta06370b

Entwistle, J. E., Beaucage, G., and Patwardhan, S. V. (2020). Mechanistic understanding of pore evolution enables high performance mesoporous silicon production for lithium-ion batteries. *J. Mater. Chem. A* 8, 4938–4949. doi: 10.1039/c9ta13633a

Favors, Z., Wang, W., Bay, H. H., Mutlu, Z., Ahmed, K., Liu, C., et al. (2014). Scalable synthesis of nano-silicon from beach sand for long cycle life li-ion batteries. *Sci. Rep.* 4:5623. doi: 10.1038/srep05623

Furquan, M., Raj Khatribail, A., Vijayalakshmi, S., and Mitra, S. (2018). Efficient conversion of sand to nano-silicon and its energetic Si-C composite anode design for high volumetric capacity lithium-ion battery. *J. Power Sources,* 382, 56–68. doi: 10.1016/j.jpowsour.2018.02.011

Galamba, N., de Castro, C. A. N., and Ely, J. F. (2004). Thermal conductivity of molten alkali halides from equilibrium molecular dynamics simulations. *J. Chem. Phys.* 120, 8676–8682.

Gao, H., Xiao, L., Plümel, I., Xu, G.-L., Ren, Y., Zuo, X., et al. (2017). Parasitic reactions in nanosized silicon anodes for lithium-ion batteries. *Nano Lett.* 17, 1512–1519.

Guo, L.-F., Zhang, S.-Y., Xie, J., Zhen, D., Jin, Y., Wan, K.-Y., et al. (2020). Controlled synthesis of nanosized Si by magnesiothermic reduction from diatomite as anode material for Li-ion batteries. *Int. J. Min. Metall. Mater.* 27, 515–525. doi: 10.1007/s12613-019-1900-z

Guo, S., Hu, X., Hou, Y., and Wen, Z. (2017). Tunable synthesis of yolk-shell porous-silicon@carbon for optimizing Si/C-based anode of lithium-ion batteries. *ACS Appl. Mater. Interfaces* 9, 42084–42092.

Gutman, I., Gotman, I., and Shapiro, M. (2006). Kinetics and mechanism of periodic structure formation at SiO2/Mg interface. *Acta Materialia* 54, 4677–4684. doi: 10.1016/j.actamat.2006.05.048

Gutman, I., Klinger, L., Gotman, I., and Shapiro, M. (2009). Model for evolution of periodic layered structure in the SiO2/Mg system. *Solid State Ion.* 180, 1350–1355. doi: 10.1016/j.ssi.2009.08.015

Han, P., Sun, W., Li, D., Luo, D., Wang, Y., Yang, B., et al. (2019). Morphology-controlled synthesis of hollow Si/C composites based on KI-assisted magnesiothermic reduction for high performance li-ion batteries. *Appl. Surf. Sci.* 481, 933–939. doi: 10.1016/j.apsusc.2019.03.051

Hieu, N. T., Suk, J., Kim, D. W., Park, J. S., and Kang, Y. (2014). Electrospun nanofibers with a core–shell structure of silicon nanoparticles and carbon nanotubes in carbon for use as lithium-ion battery anodes. *J. Mater. Chem. A* 2, 15094–15101.

Hsieh, C.-C., and Liu, W.-R. (2020). Carbon-coated Si particles binding with few-layered graphene via a liquid exfoliation process as potential anode materials for lithium-ion batteries. *Surf. Coat. Technol.* 387:125553. doi: 10.1016/j.surfcoat.2020.125553

Hsu, Y. C., Hsieh, C. C., and Liu, W. R. (2020). Synthesis of double core-shell carbon/silicon/graphite composite anode materials for lithium-ion batteries. *Surf. Coat. Technol.* 387:125528. doi: 10.1016/j.surfcoat.2020.125528

Jangid, M. K., Lakhnot, A. S., Vemulapally, A., Sonia, F. J., Sinha, S., Dusane, R. O., et al. (2018). Crystalline core amorphous shell structured silicon nanowires offer size and structure dependent reversible Na-storage.pdf>. *J. Mater. Chem. A* 6, 3422–3434. doi: 10.1039/C7TA10249F

Jia, D., Li, X., and Huang, J. (2017). Bio-inspired sandwich-structured carbon/silicon/titanium-oxide nanofibers composite as an anode material for lithium-ion batteries. *Compos. Part A Appl. Sci. Manuf.* 101, 273–282. doi: 10.1016/j.compositesa.2017.06.028

Jiang, T., Xu, X., and Chen, G. Z. (2020). Silicon prepared by electro-reduction in molten salts as new energy materials. *J. Energy Chem.* 47, 46–61. doi: 10.1016/j.jechem.2019.11.005

Kang, W., Kim, J.-C., and Kim, D.-W. (2020). Waste glass microfiber filter-derived fabrication of fibrous yolk-shell structured silicon/carbon composite freestanding electrodes for lithium-ion battery anodes. *J. Power Sour.* 468:228407. doi: 10.1016/j.jpowsour.2020.228407

Kawado, S., Maruyama, T., Suzuki, T., Isawa, N., and Hoshi, K. (1986) Crystal perfection of silicon single crystals grown by the magnetic-field-applied czochralski method. *J. Electrochem. Soc.* 133, 171–174. doi: 10.1149/1.2108515

Kierzek, K. (2016). Influence of binder adhesion ability on the performance of Silicon/Carbon Composite as Li-Ion battery anode. *J. Mater. Eng. Perform.* 25, 2326–2330. doi: 10.1007/s11665-016-2083-7

Kim, J. S., Pfleging, W., Kohler, R., Seifert, H. J., Kim, T. Y., Byun, D., et al. (2015). Three-dimensional silicon/carbon core€"shell electrode as an anode material for lithium-ion batteries. *J. Power Sour.* 279, 13–20.

Kim, Y. M., Ahn, J., Yu, S.-H., Chung, D. Y., Lee, K. J., Lee, J.-K., et al. (2015). Titanium silicide coated porous silicon nanospheres as anode materials for lithium ion batteries. *Electrochim. Acta* 151, 256–262. doi: 10.1016/j.electacta.2014.11.016

Kong, X., Zheng, Y., Wang, Y., Liang, S., Cao, G., and Pan, A. (2019). Necklace-like Si@C nanofibers as robust anode materials for high performance lithium ion batteries. *Sci. Bull.* 64, 261–269. doi: 10.1016/j.scib.2019.01.015

Kui, Z. S., Hong, W. D., Hong, Z., and Ming, M. H. (2001). The reaction between molten aluminum and silica glass. *Mater. Mech. Eng.* 25, 28–34. doi: 10.3969/j.issn.1000-3738.2001.01.010

Kumar, R., Soam, A., Dusane, R. O., and Bhargava, P. (2017). Sucrose derived carbon coated silicon nanowires for supercapacitor application. *J. Mater. Sci.* 29, 1947–1954. doi: 10.1007/s10854-017-8105-x

Li, C., Liu, C., Wang, W., Mutlu, Z., Bell, J., Ahmed, K., et al. (2017). Silicon derived from glass bottles as anode materials for lithium ion full cell batteries. *Sci. Rep.* 7:917. doi: 10.1038/s41598-017-01086-8

Li, H., Yu, H., Zhang, X., Guo, G., Hu, J., Dong, A., et al. (2016). Bowl-like 3C-SiC nanoshells encapsulated in hollow graphitic carbon spheres for high-rate lithium-ion batteries. *Chem. Mater.* 28, 1179–1186. doi: 10.1021/acs.chemmater.5b04750

Li, Q., Yin, L., Ma, J., Li, Z., Zhang, Z., Chen, A., et al. (2015). Mesoporous silicon/carbon hybrids with ordered pore channel retention and tunable carbon incorporated content as high performance anode materials for lithium-ion batteries. *Energy* 85, 159–166. doi: 10.1016/j.energy.2015.03.090

Li, X., Xing, Y., Xu, J., Deng, Q., and Shao, L. H. (2020). Uniform yolk-shell structured Si-C nanoparticles as a high performance anode material for the Li-ion battery. *Chem. Commun. (Camb.)* 56, 364–367. doi: 10.1039/c9cc07997a

Li, Y., Li, K., Liu, J., Zhang, X., Dai, J., and Ai, F. (2020). High-performance multi-layers tubular nanostructure anode materials for lithium-ion batteries. *Nano* 15:2050053. doi: 10.1142/s1793292020500538

Lim, K. W., Lee, J. I, Yang, J., Kim, Y. K., Jeong, H. Y., Park, S., et al. (2014). Catalyst-free synthesis of Si-SiOx core-shell nanowire anodes for high-rate and high-capacity lithium-ion batteries. *ACS Appl. Mater. Interfaces* 6, 6340–6345.

Lim, S., Kim, S., Ahn, K. H., and Lee, S. J. (2015). stress development of li-ion battery anode slurries during the drying process. *Ind. Eng. Chem. Res.* 54, 6146–6155. doi: 10.1021/acs.iecr.5b00878

Lin, X., Li, A., Li, D., Song, H., and Chen, X. (2020). Facile fabrication of high-performance Si/C Anode Materials via AlCl3-assisted magnesiothermic reduction of phenyl-rich polyhedral silsesquioxanes. *ACS Appl. Mater. Interfaces* 12, 15202–15210. doi: 10.1021/acsami.0c00152

Liu, J., Kopold, P., van Aken, P. A., Maier, J., and Yu, Y. (2015). Energy storage materials from nature through nanotechnology: a sustainable route from reed plants to a silicon anode for lithium-ion batteries. *Angewandte Chem. Int.* 54, 9632–9636. doi: 10.1002/anie.201503150

Liu, N., Huo, K., Mcdowell, M. T., Zhao, J., and Cui, Y. (2013). Rice husks as a sustainable source of nanostructured silicon for high performance Li-ion battery anodes. *Sci. Rep.* 3:1919.

Liu, W., Song, M. S., Kong, B., and Cui, Y. (2017). Flexible and stretchable energy storage: recent advances and future perspectives. *Adv. Mater.* 29:1603436. doi: 10.1002/adma.201603436

Liu, X., Miao, R., Yang, J., Wang, J., Bie, Y., Wang, J., et al. (2016). Scalable and cost-effective preparation of hierarchical porous silicon with a high conversion yield for superior lithium-ion storage. *Energy Technol.* 4, 593–599. doi: 10.1002/ente.201500400

Liu, X. H., Zhong, L., Huang, S., Mao, S. X., Zhu, T., and Huang, J. Y. (2012). Size-dependent fracture of silicon nanoparticles during lithiation. *ACS Nano* 6:1522.

Ma, L., Meng, J., Pan, Y., Cheng, Y. J., Ji, Q., Zuo, X., et al. (2020). Microporous binder for the silicon-based lithium-ion battery anode with exceptional rate capability and improved cyclic performance. *Langmuir* 36, 2003–2011. doi: 10.1021/acs.langmuir.9b03497

Magasinski, A., Zdyrko, B., Kovalenko, I., Hertzberg, B., Burtovyy, R., Huebner, C. F., et al. (2010). Toward efficient binders for Li-ion battery Si-based anodes: polyacrylic acid. *ACS Appl. Mater. Interfaces* 2, 3004–3010. doi: 10.1021/am100871y

McHale, A. E., Levin, E. M., and Roth, R. S. (1996). *Phase Equilibria Diagrams: Oxides*. Westerville: American Ceramic Society.

Obrovac, M., and Krause, L. (2006). Reversible cycling of crystalline silicon powder. *J. Electrochem. Soc.* 154:A103.

Obrovac, M. N., and Krause, L. J. (2007). Reversible cycling of crystalline silicon powder. *J. Electrochem. Soc.* 154, A103–A108.

Qi, Y., Wang, G., Li, S., Liu, T., Qiu, J., and Li, H. (2020). Recent progress of structural designs of silicon for performance-enhanced lithium-ion batteries. *Chem. Eng. J.* 397:125380. doi: 10.1016/j.cej.2020.125380

Qiu, D., Bu, G., Zhao, B., and Lin, Z. (2014). Mesoporous silicon microspheres fabricated via in situ magnesiothermic reduction of silicon oxide as a high-performance anode material for lithium–ion batteries. *J. Solid State Electrochem.* 19, 935–939. doi: 10.1007/s10008-014-2693-7

Rehman, W. U., Wang, H., Manj, R. Z. A., Luo, W., and Yang, J. (2019). When silicon materials meet natural sources: opportunities and challenges for low-cost lithium storage. *Small* doi: 10.1002/smll.201904508 [Epub ahead of print].

Saeedifar, Z., Nourbakhsh, A. A., Kalbasi, R. J., and Karamian, E. (2013). Low-temperature magnesiothermic synthesis of mesoporous silicon carbide from an MCM-48/Polyacrylamide nanocomposite precursor. *J. Mater. Sci. Technol.* 29, 255–260. doi: 10.1016/j.jmst.2013.01.007

Sainan, L., Qiang, Z., Huaming, Y., Dawei, M., Anqiang, P., and Shuquan, L. (2018). Fabrication of Si Nanoparticles@Carbon fibers composites from natural nanoclay as an advanced lithium-ion battery flexible anode. *Minerals* 8:180.

Shepherd, R. F., Panda, P., Bao, Z., Sandhage, K. H., Hatton, T. A., Lewis, J. A., et al. (2008). Stop−Flow lithography of colloidal, glass, and silicon microcomponents. *Adv. Mater.* 20, 4734–4739. doi: 10.1002/adma.200801090

Shi, L., Wang, W., Wang, A., Yuan, K., and Yang, Y. (2016). Understanding the impact mechanism of the thermal effect on the porous silicon anode material preparation via magnesiothermic reduction. *J. Alloys Compounds* 661, 27–37. doi: 10.1016/j.jallcom.2015.11.196

Shivaraju, G. C., Sudakar, C., and Prakash, A. S. (2019). High-rate and long-cycle life performance of nano-porous nano-silicon derived from mesoporous MCM-41 as an anode for lithium-ion battery. *Electrochim. Acta* 294, 357–364. doi: 10.1016/j.electacta.2018.10.122

Sohn, M., Lee, D. G., Park, H. I., Park, C., Choi, J. H., and Kim, H. (2018). Microstructure controlled porous silicon particles as a high capacity lithium storage material via dual step pore engineering. *Adv. Funct. Mater.* 28:1800855.

Sola-Rabada, A., Sahare, P., Hickman, G. J., Vasquez, M., Canham, L. T., Perry, C. C., et al. (2018). Biogenic porous silica and silicon sourced from Mexican Giant Horsetail (*Equisetum myriochaetum*) and their application as supports for enzyme immobilization. *Colloids Surf. B Biointerfaces* 166, 195–202. doi: 10.1016/j.colsurfb.2018.02.047

Stetson, C., Yin, Y., Jiang, C. S., Decaluwe, S. C., and Burrell, A. K. (2019). Temperature-dependent solubility of solid electrolyte interphase on silicon electrodes. *ACS Energy Lett.* 4, 2770–2775.

Stöber, W., Fink, A., and Bohn, E. (1968). Controlled growth of monodisperse silica spheres in the micron size range. *J. Colloid Interface Sci.* 26, 62–69.

Sun, Y., Liu, N., and Cui, Y. (2016). Promises and challenges of nanomaterials for lithium-based rechargeable batteries. *Nat. Energy* 1, 16071. doi: 10.1038/nenergy.2016.71

Taeseup, S., Jianliang, X., Jin-Hyon, L., Dong Hyun, L., Keh-Chih, H., John, A. R., et al. (2010). Arrays of sealed silicon nanotubes as anodes for lithium ion batteries. *Nano Lett.* 10, 1710–1716.

Tang, X., Wen, G., and Song, Y. (2018). Novel scalable synthesis of porous silicon/carbon composite as anode material for superior lithium-ion batteries. *J. Alloys Compounds* 739, 510–517. doi: 10.1016/j.jallcom.2017.12.331

Tao, H.-C., Huang, M., Fan, L.-Z., and Qu, X. (2012). Interweaved Si@SiOx/C nanoporous spheres as anode materials for Li-ion batteries. *Solid State Ionics* 220, 1–6. doi: 10.1016/j.ssi.2012.05.014

Teng, Z., Zheng, G., Dou, Y., Li, W., Mou, C. Y., Zhang, X., et al. (2012). Highly ordered mesoporous silica films with perpendicular mesochannels by a simple stöber-solution growth approach. *Angew. Chem. Int. Edition* 51, 2173–2177.

Terranova, M. L., Orlanducci, S., Tamburri, E., Guglielmotti, V., and Rossi, M. (2014). Si/C hybrid nanostructures for Li-ion anodes: an overview. *J. Power Sour.* 246, 167–177. doi: 10.1016/j.jpowsour.2013.07.065

Tornheim, A., Trask, S. E., and Zhang, Z. (2019). Communication—effect of lower cutoff voltage on the 1st cycle performance of silicon electrodes. *J. Electrochem. Soc.* 166:A132.

Waitzinger, M., Elsaesser, M. S., Berger, R. J. F., Akbarzadeh, J., Peterlik, H., and Hüsing, N. (2015). Self-supporting hierarchically organized silicon networks via magnesiothermic reduction. *Monatshefte Chem.* 147, 269–278. doi: 10.1007/s00706-015-1611-8

Wang, H., Xu, H., Jia, K., and Wu, R. (2018). ZIF-8-Templated Hollow Cubelike Si/SiO2@C nanocomposites for superior lithium storage performance. *ACS Appl. Energy Mater.* 2, 531–538. doi: 10.1021/acsaem.8b01553

Wang, J., Lü, H.-Y., Fan, C.-Y., Wan, F., Guo, J.-Z., Wang, Y.-Y., et al. (2017). Ultrafine nano-Si material prepared from NaCl-assisted magnesiothermic reduction of scalable silicate: graphene-enhanced Li-storage properties as advanced anode for lithium-ion batteries. *J. Alloys Compounds* 694, 208–216. doi: 10.1016/j.jallcom.2016.09.323

Wissel, K., Vrankovic, D., Trykowski, G., and Graczyk-Zajac, M. (2017). Synthesis of 3D silicon with tailored nanostructure: Influence of morphology on the electrochemical properties. *Solid State Ionics* 302, 180–185. doi: 10.1016/j.ssi.2016.12.008

Won, C. W., Nersisyan, H. H., and Won, H. I. (2011). Solar-grade silicon powder prepared by combining combustion synthesis with hydrometallurgy. *Solar Energy Mater. Solar Cells* 95, 745–750. doi: 10.1016/j.solmat.2010.10.016

Wu, L., Yang, J., Tang, J., Ren, Y., Nie, Y., and Zhou, X. (2016). Three-dimensional graphene nanosheets loaded with Si nanoparticles by in situ reduction of SiO2 for lithium ion batteries. *Electrochim. Acta* 190, 628–635. doi: 10.1016/j.electacta.2015.12.192

Xie, J., Wang, G., Huo, Y., Zhang, S., Cao, G., and Zhao, X. (2014). Nanostructured silicon spheres prepared by a controllable magnesiothermic reduction as anode for lithium ion batteries. *Electrochim. Acta* 135, 94–100. doi: 10.1016/j.electacta.2014.05.012

Xing, Z., Lu, J., and Ji, X. (2018). A brief review of metallothermic reduction reactions for materials preparation. *Small Methods* 2:1800062. doi: 10.1002/smtd.201800062

Yan, Z., and Guo, J. (2019). High-performance silicon-carbon anode material via aerosol spray drying and magnesiothermic reduction. *Nano Energy* 63:103845. doi: 10.1016/j.nanoen.2019.06.041

Yang, J., Wang, Y., Chou, S., Zhang, R., Xu, Y., Fan, J., et al. (2015). Yolk-shell silicon-mesoporous carbon anode with compact solid electrolyte interphase film for superior lithium-ion batteries. *Nano Energy* 18, 133–142.

Yang, Z., Du, Y., Hou, G., Ouyang, Y., Ding, F., and Yuan, F. (2020). Nanoporous silicon spheres preparation via a controllable magnesiothermic reduction as anode for Li-ion batteries. *Electrochim. Acta* 329:135141. doi: 10.1016/j.electacta.2019.135141

Yao, Y., Mcdowell, M. T., Ryu, I., Wu, H., Liu, N., Hu, L., et al. (2011). Interconnected silicon hollow nanospheres for lithium-ion battery anodes with long cycle life. *Nano Lett.* 11, 2949–2954.

Yoo, J.-K., Kim, J., Choi, M.-J., Park, Y.-U., Hong, J., Baek, K. M., et al. (2014). Extremely high yield conversion from low-cost sand to high-capacity si electrodes for li-ion batteries. *Adv. Energy Mater.* 4:1400622. doi: 10.1002/aenm.201400622

Yoshikawa, T., and Morita, K. (2012). An evolving method for solar-grade silicon production: solvent refining. *JOM* 64, 946–951. doi: 10.1007/s11837-012-0371-8

Yu, K., Zhang, H., Qi, H., Gao, X., Liang, J., and Liang, C. (2018). Rice husk as the source of silicon/carbon anode material and stable electrochemical performance. *ChemistrySelect* 3, 5439–5444. doi: 10.1002/slct.201800650

Zakaryan, M. K., Aydinyan, S. V., and Kharatyan, S. L. (2017). Preparation of fine-grained silicon from serpentine mineral by magnesiothermic reduction of silica in the presence of reaction products as diluents. *Silicon* 9, 841–846. doi: 10.1007/s12633-017-9583-4

Zhang, R., Du, Y., Li, D., Shen, D., Yang, J., Guo, Z., et al. (2014). Highly reversible and large lithium storage in mesoporous si/c nanocomposite anodes with silicon nanoparticles embedded in a carbon framework. *Adv. Mater.* 26, 6749–6755. doi: 10.1002/adma.201402813

Zhang, Y., Hu, K., Zhou, Y., Xia, Y., Yu, N., Wu, G., et al. (2019). A facile, one-step synthesis of silicon/silicon carbide/carbon nanotube nanocomposite as a cycling-stable anode for lithium ion batteries. *Nanomaterials (Basel)* 9:1624. doi: 10.3390/nano9111624

Zhang, Y.-C., You, Y., Xin, S., Yin, Y.-X., Zhang, J., Wang, P., et al. (2016). Rice husk-derived hierarchical silicon/nitrogen-doped carbon/carbon nanotube spheres as low-cost and high-capacity anodes for lithium-ion batteries. *Nano Energy* 25, 120–127. doi: 10.1016/j.nanoen.2016.04.043

Zhang, Z., and Li, H. (2020). Sequential-template synthesis of hollowed carbon polyhedron@SiC@Si for lithium-ion battery with high capacity and electrochemical stability. *Appl. Surface Sci.* 514:145920. doi: 10.1016/j.apsusc.2020.145920

Zhang, Z., Wong, L. M., Wang, H. X., Wei, Z. P., Zhou, W., Wang, S. J., et al. (2010). Self-assembled in-plane growth of Mg2SiO4 nanowires on Si substrates catalyzed by Au nanoparticles. *Adv. Funct. Mater.* 20, 2511–2518. doi: 10.1002/adfm.201000442

Zhao, Z., Xie, H., Qu, J., Zhao, H., Ma, Q., Xing, P., et al. (2019). A natural transporter of silicon and carbon: conversion of rice husks to silicon carbide or carbon−silicon hybrid for lithium−ion battery anodes via a molten salt electrolysis approach. *Batter. Supercaps* 2, 1007–1015. doi: 10.1002/batt.201900091

Zhilkashinova, A. M., Kabdrakhmanova, S. K., Troyeglazova, A. V., and Abilev, M. B. (2018). Structure and properties of metallurgical-grade silicon. *Silicon* 10, 2201–2210.

Zhou, X., Wu, L., Yang, J., Tang, J., Xi, L., and Wang, B. (2016). Synthesis of nano-sized silicon from natural halloysite clay and its high performance as anode for lithium-ion batteries. *J. Power Sour.* 324, 33–40. doi: 10.1016/j.jpowsour.2016.05.058

Zhu, J., Ren, Y., Yang, B., Chen, W., and Ding, J. (2017). Embedded Si/graphene composite fabricated by magnesium-thermal reduction as anode material for lithium-ion batteries. *Nanoscale Res. Lett.* 12:627. doi: 10.1186/s11671-017-2400-6

Zuo, X., Wang, X., Xia, Y., Yin, S., Ji, Q., Yang, Z., et al. (2019). Silicon/carbon lithium-ion battery anode with 3D hierarchical macro-/mesoporous silicon network: self-templating synthesis via magnesiothermic reduction of silica/carbon composite. *J. Power Sour.* 412, 93–104. doi: 10.1016/j.jpowsour.2018.11.039

Conflict of Interest: The authors declare that the research was conducted in the absence of any commercial or financial relationships that could be construed as a potential conflict of interest.